Accepted Manuscript

1-Aryl-1*H*- and 2-aryl-2*H*-1,2,3-triazole derivatives blockade P2X7 receptor *in vitro* and inflammatory response *in vivo*

Daniel Tadeu Gomes Gonzaga, Leonardo Braga Gomes Ferreira, Thadeu Estevam Moreira Maramaldo Costa, Natalia Lidmar von Ranke, Paulo Anastácio Furtado Pacheco, Ana Paula Sposito Simões, Juliana Carvalho Arruda, Luiza Pereira Dantas, Hércules Rezende de Freitas, Ricardo Augusto de Melo Reis, Carmen Penido, Murilo Lamim Bello, Helena Carla Castro, Carlos Rangel Rodrigues, Vitor Francisco Ferreira, Robson Xavier Faria, Fernando de Carvalho da Silva

PII: S0223-5234(17)30637-2

DOI: 10.1016/j.ejmech.2017.08.034

Reference: EJMECH 9678

To appear in: *European Journal of Medicinal Chemistry*

Received Date: 5 May 2017

Revised Date: 2 August 2017

Accepted Date: 15 August 2017

Please cite this article as: D.T.G. Gonzaga, L.B.G. Ferreira, T.E. Moreira Maramaldo Costa, N.L. von Ranke, P. Anastácio Furtado Pacheco, A.P. Sposito Simões, J.C. Arruda, L.P. Dantas, Hé.Rezende. de Freitas, R.A. de Melo Reis, C. Penido, M.L. Bello, H.C. Castro, C.R. Rodrigues, V.F. Ferreira, R.X. Faria, F.d.C. da Silva, 1-Aryl-1*H*- and 2-aryl-2*H*-1,2,3-triazole derivatives blockade P2X7 receptor *in vitro* and inflammatory response *in vivo*, *European Journal of Medicinal Chemistry* (2017), doi: 10.1016/j.ejmech.2017.08.034.

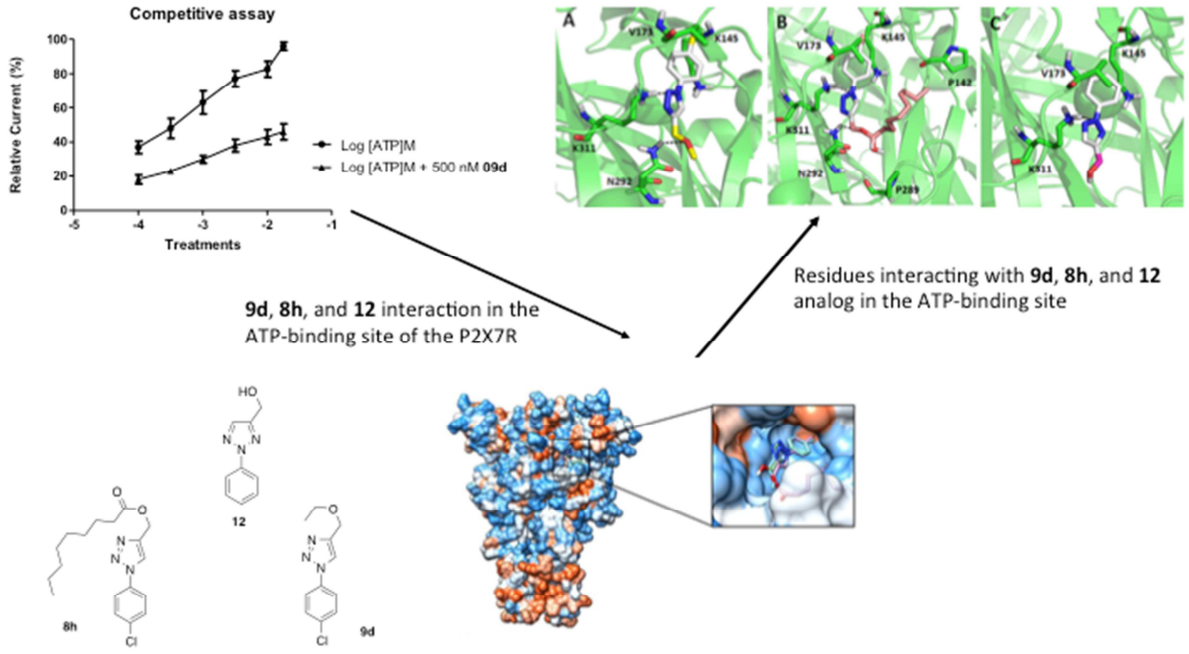

1-Aryl-1*H*- and 2-aryl-2*H*-1,2,3-triazole derivatives blockade P2X7 receptor *in vitro* and inflammatory response *in vivo*

Daniel Tadeu Gomes Gonzaga,[a,b] Leonardo Braga Gomes Ferreira,[c] Thadeu Estevam Moreira Maramaldo Costa,[d,e] Natalia Lidmar von Ranke,[f,g] Paulo Anastácio Furtado Pacheco,[h] Ana Paula Sposito Simões,[h] Juliana Carvalho Arruda,[h] Luiza Pereira Dantas,[h] Hércules Rezende de Freitas,[i] Ricardo Augusto de Melo Reis,[i] Carmen Penido,[d,e] Murilo Lamim Bello,[g] Helena Carla Castro,[f] Carlos Rangel Rodrigues,[g] Vitor Francisco Ferreira,[b] Robson Xavier Faria,[h,*] Fernando de Carvalho da Silva[b,*]

[a] Fundação Oswaldo Cruz, Instituto de Tecnologia em Fármacos, Farmanguinhos - Fiocruz, Departamento de Síntese de Fármacos Manguinhos, CEP 21041-250, Rio de Janeiro-RJ, Brazil.

[b] Universidade Federal Fluminense, Departamento de Química Orgânica, Instituto de Química, Campus do Valonguinho, CEP 24020-150, Niterói-RJ, Brazil.

[c] Fundação Oswaldo Cruz, Instituto Oswaldo Cruz, Laboratório de Inflamação, Avenida Brasil 4365, Manguinhos, CEP 21045-900, Rio de Janeiro-RJ, Brazil.

[d] Fundação Oswaldo Cruz, Laboratório de Farmacologia Aplicada, Farmanguinhos - Fiocruz, CEP 21041-250, Rio de Janeiro-RJ, Brazil.

[e] Fundação Oswaldo Cruz, Centro de Desenvolvimento Tecnológico em Saúde, Instituto Nacional de Ciência e Tecnologia de Inovação em Doenças Negligenciadas (INCT-IDN), Rio de Janeiro-RJ, Brazil.

[f] Universidade Federal Fluminense, Laboratório de Antibióticos, Bioquímica, Ensino e Modelagem Molecular – LABiEMol, CEP 24020-150, Brazil.

[g] Universidade Federal do Rio de Janeiro, Faculdade de Farmácia, Departamento de Fármacos e Medicamentos, Laboratório de Modelagem Molecular e QSAR - ModMolQSAR, CEP 21941-902, RJ, Brazil.

[h] Fundação Oswaldo Cruz, Instituto Oswaldo Cruz, Laboratório de Toxoplasmose e outras Protozooses, Avenida Brasil 4365, Manguinhos, CEP 21045-900, Rio de Janeiro-RJ, Brazil.

[i] Universidade Federal do Rio de Janeiro, Instituto de Biofísica, Laboratório de Neuroquímica, CEP 21941-902, RJ, Brazil.

Corresponding authors

Chemistry: Fernando de Carvalho da Silva, Universidade Federal Fluminense, Departamento de Química Orgânica, Instituto de Química, Campus do Valonguinho, CEP 24020-150, Niterói-RJ, Brazil; E-mail: gqofernando@vm.uff.br

Pharmacology: Robson Xavier Faria, Fundação Oswaldo Cruz, Instituto Oswaldo Cruz, Laboratório de Comunicação Celular, Avenida Brasil 4365, Manguinhos, CEP 21045-900 - Rio de Janeiro-RJ, Brazil.; E-mail: robson.xavier@gmail.com

***Both authors contributed equally to this work.**

Abbreviations

ATP, adenosine 5′-triphosphate; HEPES, 4-(2-hydroxyethyl)-1-piperazineethanesulfonic acid; ELISA, enzyme-linked immunosorbent assay; SDS, sodium dodecyl sulfate; IC_{50}, half-maximum inhibitory concentration; IL, interleukin; LPS, lipopolysaccharide; ESI, electrospray ionization; NMR, nuclear magnetic resonance, LDH, lactate dehydrogenase; EGTA, ethylene glycol tetraacetic acid; PBS, phosphate-buffered saline; NAD^+, Nicotinamide adenine dinucleotide; IL-1β, Interleukin 1β; PI, Propidium iodide; BBG, Brilliant Blue G; DMEM, Dulbecco's Modified Eagle's Medium; IR, infrared spectroscopy; TMS, tetramethylsilane; TLC, Thin Layer Chromatography; ROS, Reactive oxygen species; iNOS, inducible nitric oxide synthase; PPADS (pyridoxalphosphate-6-azophenyl-2',4'-disulfonic acid); A740003, *N*-[1-[[(Cyanoamino)(5-quinolinylamino)methylene]amino]-2,2-dimethylpropyl]-3,4-dimethoxybenzeneacetamide; A804598, AZ 10606120 dihydrochloride, *N*-Cyano-*N*''-[(1*S*)-1-phenylethyl]-*N*'-5-quinolinyl-guanidine; *N*-[2-[[2-[(2-Hydroxyethyl)amino]ethyl]amino]-5-quinolinyl]-2-tricyclo[3.3.1.13,7]dec-1-ylacetamide dihydrochloride; A438079, 3-[[5-(2,3-Dichlorophenyl)-1*H*-tetrazol-1-yl]methyl]pyridine hydrochloride; AZ11645373, 3-[1-[[(3'-Nitro[1,1'-biphenyl]-4-yl)oxy]methyl]-3-(4-pyridinyl)propyl]-2,4-thiazolidinedione; THP-1 cell, human monocytic cell line derived from an acute monocytic leukemia patient; and SAR, Structure-activity relationship.

Abstract: Fifty-one 1,2,3-triazole derivatives were synthesized and evaluated with respect to P2X7 receptor (P2X7R) activity and its associated pore. These triazoles were screened *in vitro* for dye uptake assay and its cytotoxicity against mammalian cell types. Seven 1,2,3-triazole derivatives (**5e**, **6e**, **8h**, **9d**, **9i**, **11**, and **12**) potently blocked P2X7 receptor pore formation *in vitro* (J774.G8 cells and peritoneal macrophages). All blockers displayed IC_{50} value inferior to 500 nM, and they have low toxicity in either cell types. These seven selected triazoles inhibited P2X7R mediated interleukin-1 (IL-1β) release. In particular, compound **9d** was the most potent P2X7R blocker. Additionally, in mouse acute models of inflammatory responses induced by ATP or carrageenan administration in the paw, compound **9d** promoted a potent blocking response. Similarly, **9d** also reduced mouse LPS-induced pleurisy cellularity. *In silico* predictions indicate this molecule appropriate to develop an anti-inflammatory agent when it was compared to commercial analogs. Electrophysiological studies suggest a competitive mechanism of action of **9d** to block P2X7 receptor. Molecular docking was performed on the ATP binding site in order to observe the preferential interaction pose, indicating that binding mode of the **9d** is by interacting its 1,2,3-triazole and ether moiety with positively charged residues and with its chlorobenzene moiety orientated toward the apolar end of the ATP binding site which are mainly composed by the Ile170, Trp167 and Leu309 residues from α subunit. These results highlight **9d** derivative as a drug candidate with potential therapeutic application based on P2X7 receptor blockade.

Keywords: Purinergic receptors; antagonist; anti-inflammatory; synthetic products; ATP; pore formation.

1. Introduction

The physiology and pharmacology of the ligand-gated P2X family of ion channels have been studied broadly in terms of their biophysical, pharmacological and physiological aspects [1-4]. As a function of its wide expression in cells of hematopoietic origin, the ATP-sensitive P2X7 receptor (P2X7R) has acquired a respectable amount of attention because recent data suggest that it has a role in acute and chronic inflammation [5-8].

P2X7R is found on native or cell lineages of macrophages [9-12]. Activation of P2X7R with extracellular ATP promotes ion flux [13] and the formation of a reversible cell membrane pore that is associated with lysis and cell death [14-16]. In addition, this receptor has also been linked to inflammatory conditions that activate and release interleukin-1 β [17,18], among other substances, such as glutamate [19].

The cooperation between P2X7R stimulation of glutamate metabolism and cytokines is part of the functional rationale for its action in the amelioration and progression of important disorder states or conditions involving inflammation [20], neurodegeneration [21], and neuropathic pain [22,23]. In the P2X7 knockout mice, there is a decrease in the development of inflammatory and neuropathic pain and rigor symptoms in an arthritis model [24,25].

Although there are a large number of P2X7R antagonists commercially available, research of novel molecules with antagonist and therapeutic action on this receptor is necessary. First-generation P2X7R antagonists (Suramin, PPADS, BBG, KN-62 and Reactive blue-2) are non-selective inhibitors, acting also on other P2Rs [26] or in proteins related to P2X7R pore formation mechanism [6]. The second generation of P2X7R antagonists includes JNJ-47965567 [27], A740003 [28], GSK314181 [29], triazole derivatives A438079 [30], A839977 [31], AZ11645373 [81], AZ10606120 [32] and AZD9056 [33]. Characterization of their mechanisms of action and pharmacologic properties *in vivo* are largely unknown. In some cases, they exhibit reduced availability and variable potency according to the species studied [26].

Clinical trials using P2X7R antagonists against rheumatoid arthritis indicated clinical efficacy and safety of the P2X7R antagonists AZD9056 or CE-224,535 [33,34]. In contrast, both trials did not exhibit therapeutic benefit [80,81]. A possible explanation is associated to studies related to differential pharmacological sensibility in P2X7R genotype function, as observed by McHugh and collaborators *in vitro* [35]. This scenario leaves open a possibility to search and develop novel P2X7R antagonists.

Numerous types of P2X7R antagonists have been identified [36,37], however most are inappropriate for therapeutic use. In recent years, our scientific group has concentrated on making P2X7R antagonist molecular low weight compounds for treating inflammation and pain. In this context, the 1,2,3-triazoles are synthetic five members heterocyclic aromatic compounds containing three nitrogen atoms [38]. These compounds have diverse biological activities [39] such as anti-HIV [40], β-lactamase inhibitors [41], antiepileptic activities [42], anti-platelet agents [43,44], dopamine D2 receptor ligands (related to Schizophrenia) [45], anti-inflammatory [46], antimicrobial [47-50], anti-herpes simplex virus (HSV) [51], trypanocidal [52], antileishmanial agents [53], antifungal agents [54] and glycosidase inhibitors [55,56].

Some heterocyclic compounds containing 1,2,3-triazole structure core have been described as P2X7R antagonists [57,58]. In 2007, Carrol and colleagues promoted substitutions in a tetrazole core inserting triazole isostere. Triazole-based P2X7 antagonists showed potency (pIC_{50} 6.43-7.12) and physiochemical properties improved in comparison to tetrazole analogues [59]. Based on assays above, Florjancic and collaborates used SARs to search the aminotriazole activity at both human

and rat P2X7R. In consequence, they observed drugs with pIC_{50} value in turn of 7.5 to block both receptors [60].

Honore [31] demonstrated *in vitro* and *in vivo* the inhibitory activity of a structurally novel P2X7R antagonist, 1-(2, 3-dichlorophenyl)-*N*-[2-(pyridin-2-yloxy) benzyl]-1*H*-tetrazol-5-amine (A-839977) in mice. A-839977 inhibited BzATP-evoked calcium influx at recombinant human, rat and mouse P2X7Rs. The IC_{50} values varied from 20-150 nM for Ca^{2+} assay, $pIC_{50} = 8.18 \pm 0.03$ for dye uptake and $pIC_{50} = 7.43 \pm 0.13$ to IL-1β release assay.

However, phenyl triazoles were not test against P2X7R antagonistic activity. Then, the aim of this study was to evaluate the blocking action and cytotoxicity of 1-Phenyl-1*H*- and 2-phenyl-2*H*-1,2,3-triazol derivatives (Fig. 2) on P2X7R activity and its associated pore.

2. Experimental Section

2.1. Chemistry

The reagents were purchased from Sigma-Aldrich Brazil and were used without further purification. Column chromatography was performed with silica gel 60 (Merck 70-230 mesh). Analytical thin layer chromatography was performed with silica gel plates (Merck, TLC silica gel 60 F254), and the plots were visualized using UV light or aqueous solutions of ammonium sulfate. The indicated yields refer to chromatographically and spectroscopically homogeneous materials. Melting points were obtained on a Fischer-Johns apparatus and were uncorrected. Infrared spectra were measured with KBr pellets on a Perkin-Elmer model 1420 FT-IR Spectrophotometer, and the spectra were calibrated relative to the 1601.8 cm^{-1} absorbance of polystyrene. NMR spectra were recorded on a Varian Unity Plus VXR (500 MHz) instrument in DMSO-d_6 or $CDCl_3$ solutions. The chemical shift data were reported in units of d (ppm) downfield from tetramethylsilane or the solvent, either of which was used as an internal standard; coupling constants (*J*) are reported in hertz and refer to apparent peak multiplicities. CHN elemental analyses were performed on a Perkin-Elmer 2400 CHN elemental analyzer.

2.1.1. General procedure for preparing 1,2,3-triazoles

The protocols for preparing all of the 1,2,3-triazoles and the physical and spectroscopic data for **5a-e**, **6a-b**, **7a**, **8a-k**, **9a**, **9c-d**, **9f**, **9i-n**, **10**, **11**, **12**, **13a-d**, **14a** and **14c** were previously reported in our studies [47,56].

*2.1.1.1. 1-(4-methoxyphenyl)-1H-1,2,3-triazole-4-carbaldehyde (**6c**).* Brown solid, 84% yield; m.p. 131-132ºC; IR (KBr, cm^{-1}): ν 3133, 2969, 1688, 1607, 1518, 1459, 1299, 1255, 1206, 1168, 1027, 827, 777, 614; ^{1}H NMR (DMSO-d_6, 500 MHz): 3.96 (3H, s), 7.27-7.30 (2H, m), 7.98-8.02 (2H, m), 9.55 (1H, s), 10.22 (1H, s); ^{13}C NMR (DMSO-d_6, 125 MHz APT): 55.7, 115.0, 122.4, 125.9, 129.3, 147.5, 159.9, 184.9.

*2.1.1.2. 1-(3,5-dichlorophenyl)-1H-1,2,3-triazole-4-carbaldehyde oxime (**7b**).* White solid, 52% yield; m.p. 111-112ºC; IR (KBr, cm^{-1}): ν 3098, 1588, 1477, 1437, 1337, 1234, 1122, 1053, 987, 932, 854, 812, 695, 665; ^{1}H NMR (DMSO-d_6, 500 MHz): 7.89 (1H, t, *J* 2.0 Hz), 7.88 (2H, d, *J* 2.0 Hz), 8.36 (1H, s), 9.30 (1H, s), 11.63 (1H, s); ^{13}C NMR (DMSO-d_6, 125 MHz APT): δ 118.9, 120.9, 128.2, 135.2, 138.0, 139.8, 142.6. Anal. Calcd for $C_9H_6Cl_2N_4O$: C, 42.05; H, 2.35; N, 21.79. Found: C, 41.95; H, 2.45; N, 21.65.

*2.1.1.3. (1-(2,5-dichlorophenyl)-1H-1,2,3-triazol-4-yl)methyl nonanoate (**8l**).* White solid, 95% yield; m.p. 35-36ºC; IR (KBr, cm^{-1}): ν 3664, 2919, 2852, 1741, 1588, 1489, 1451, 1377, 1285, 1252, 1210, 1168, 1102, 1074, 1043, 1018, 874, 822, 722, 651; ^{1}H NMR (DMSO-d_6, 500 MHz): 0.97 (3H, t, *J* 7.0 Hz), 1.30-1.41 (12H, m), 1.59-1.67 (2H, m), 2.46 (2H, t, *J* 7.0 Hz), 5.36 (2H, s), 7.85 (2H, dd, *J* 2.0 and 8.0 Hz), 7.93 (1H, d, *J* 8.0 Hz), 8.01 (1H, d, *J* 2.0 Hz), 8.42 (1H, s); ^{13}C NMR (DMSO-d_6, 125 MHz APT): δ 13.9, 22.0, 24.4, 28.4, 28.6, 28.8, 31.3, 33.4, 33.7, 56.7, 126.7, 127.5, 128.1, 131.5, 131.9, 132.5, 135.3, 142.3, 172.6. Anal. Calcd for $C_{19}H_{25}Cl_2N_3O_2$: C, 57.29; H, 6.33; N, 10.55. Found: C, 57.00; H, 6.25; N, 10.65.

*2.1.1.4. (1-(3,5-dichlorophenyl)-1H-1,2,3-triazol-4-yl)methyl benzoate (**8m**).* Brown solid, 40% yield; m.p. 85-86ºC; IR (KBr, cm^{-1}): ν 3149, 3089, 1707, 1584, 1484, 1451, 1277, 1108, 1053, 1013, 970, 855, 804, 712, 665; ^{1}H NMR (DMSO-d_6, 500 MHz): 5.63 (2H, s), 7.64-7.68 (2H, m), 7.78-7.81 (1H, m), 7.87 (1H, t, *J* 2.0 Hz), 8.12-8.14 (2H, m), 8.21 (2H, d, *J* 2.0 Hz), 9.20 (1H, s); ^{13}C NMR (DMSO-d_6, 125 MHz APT): 57.8, 118.8, 123.3, 128.1, 128.8, 129.3, 129.3, 133.5, 135.2, 138.1, 143.5, 165.4. Anal. Calcd for $C_{16}H_{11}Cl_2N_3O_2$: C, 55.19; H, 3.18; N, 12.07. Found: C, 55.35; H, 3.08; N, 12.02.

*2.1.1.5. (1-(3,5-dichlorophenyl)-1H-1,2,3-triazol-4-yl)methyl acetate (**8n**).* Brown solid, 87% yield; m.p. 74-75ºC; IR (KBr, cm^{-1}): ν 3136, 3096, 2361, 1710, 1588, 1477, 1439, 1387, 1367, 1284,

1238, 1120, 1023, 990, 951, 899, 856, 831, 795, 670, 638; ^{1}H NMR (DMSO-d_6, 500 MHz): 2.20 (3H, s), 5.34 (2H, s), 7.87 (1H, t, *J* 2.0 Hz), 8.19 (2H, d, *J* 2.0 Hz), 9.09 (1H, s); ^{13}C NMR (DMSO-d_6, 125 MHz APT): 20.6, 56.9, 118.7, 123.2, 128.1, 135.3, 138.1, 143.6, 170.1. Anal. Calcd for $C_{11}H_9Cl_2N_3O_2$: C, 46.18; H, 3.17; N, 14.69. Found: C, 46.06; H, 3.08; N, 14.32.

*2.1.1.6. (1-(4-methoxyphenyl)-1H-1,2,3-triazol-4-yl)methyl benzoate (**8o**)*. White solid, 65% yield; m.p. 95-96ºC; IR (KBr, cm^{-1}): ν 3126, 2921, 1708, 1599, 1518, 1448, 1379, 1268, 1189, 1099, 1035, 941, 824, 771, 708; ^{1}H NMR (DMSO-d_6, 500 MHz): 3.95 (3H, s), 5.61 (2H, s), 7.25-7.26 (2H, m), 7.65 (2H, m), 7.79 (1H, m), 8.11-8.13 (2H, m), 8.95 (1H, s); ^{13}C NMR (DMSO-d_6, 125 MHz APT): 55.6, 57.9, 114.9, 121.9, 123.0, 128.8, 129.3, 129.4, 130.0, 133.5, 142.9, 159.4, 165.5. Anal. Calcd for $C_{17}H_{15}N_3O_3$: C, 66.01; H, 4.89; N, 13.58. Found: C, 66.21; H, 4.85; N, 13.60.

*2.1.1.7. (1-(4-methoxyphenyl)-1H-1,2,3-triazol-4-yl)methyl acetate (**8p**)*. Brown solid, 82% yield; m.p. 60-61ºC; IR (KBr, cm^{-1}): ν 3143, 1722, 1610, 1517, 1440, 1375, 1303, 1247, 1191, 1111, 1027, 976, 921, 829, 759, 632; ^{1}H NMR (DMSO-d_6, 500 MHz): 2.18 (3H, s), 3.95 (3H, s), 5.32 (2H, s), 7.24-7.27 (2H, m), 7.90-7.93 (2H, m), 8.83 (1H, s); ^{13}C NMR (DMSO-d_6, 125 MHz APT): 20.6, 55.5, 57.0, 114.9, 121.8, 122.8, 130.0, 142.9, 159.4, 170.1. Anal. Calcd for $C_{12}H_{13}N_3O_3$: C, 58.29; H, 5.30; N, 16.99. Found: C, 58.49; H, 5.25; N, 16.89.

*2.1.1.8. (1-(4-methoxyphenyl)-1H-1,2,3-triazol-4-yl)methyl pentanoate (**8q**)*. Yellow oil, 55% yield; IR (KBr, cm^{-1}): ν 2932, 2870, 1734, 1611, 1518, 1462, 1304, 1253, 1164, 1109, 1034, 989, 832, 770; ^{1}H NMR (DMSO-d_6, 500 MHz): 0.96 (3H, t, *J* 7.4 Hz), 1.35-1.40 (4H, m), 1.52 (2H, p, *J* 7.4 Hz), 2,45 (2H, t, *J* 7.4 Hz), 3.95 (3H, s), 5.33 (2H, s), 7.25 (2H, d, *J* 9.0 Hz), 7.91 (2H, d, *J* 9.0 Hz), 8.82 (1H, s); ^{13}C NMR (DMSO-d_6, 125 MHz APT): 13.7, 21.7, 24.1, 30.6, 33.3, 55.6, 56.9, 114.9, 121.8, 122.8, 130.0, 142.9, 159.4, 172.6. Anal. Calcd for $C_{16}H_{21}N_3O_3$: C, 63.35; H, 6.98; N, 13.85. Found: C, 63.05; H, 7.12; N, 13.89.

*2.1.1.9. 1-phenyl-4-(propoxymethyl)-1H-1,2,3-triazole (**9b**)*. Yellow oil, 62% yield; IR (KBr, cm^{-1}): ν 2961, 2933, 2872, 1730, 1598, 1503, 1465, 1377, 1339, 1229, 1095, 1040, 989, 814, 757, 690; ^{1}H NMR (DMSO-d_6, 500 MHz): 0.87 (3H, t, *J* 7.0 Hz), 1.54 (2H, sex, *J* 7.0 Hz), 3.45 (2H, t, *J* 7.0 Hz), 4.58 (2H, s), 7.75 (1H, t, *J* 7.7 Hz), 7.59 (2H, t, *J* 7.7 Hz), 7.89 (2H, d, *J* 7.7 Hz), 8.76 (1H, s); ^{13}C NMR (DMSO-d_6, 125 MHz APT): 10.6, 22.5, 63.3, 71.5, 120.2, 122.2, 128.8, 130.0, 136.8, 145,6. Anal. Calcd for $C_{12}H_{15}N_3O$: C, 66.34; H, 6.96; N, 19.34. Found: 66.54; H, 7.12; N, 18.89.

*2.1.1.10. 1-(4-chlorophenyl)-4-(propoxymethyl)-1H-1,2,3-triazole (**9e**).* Yellow solid, 45% yield; m.p. 75-76 ºC; IR (KBr, cm^{-1}): ν 3160, 2968, 2932, 2871, 1721, 1563, 1502, 1456, 1341, 1229, 1194, 1092, 984, 954, 837, 817, 783, 737, 697, 753; ^{1}H NMR (DMSO-d_6, 500 MHz): 0.99 (3H, t, *J* 7.0 Hz), 1.66 (2H, sex, *J* 7.0 Hz), 3.56 (2H, t, *J* 7,0 Hz), 4.70 (2H, s), 7.77-7.79 (2H, m), 8.05-8.07 (2H, m), 8.90 (1H, s); ^{13}C NMR (DMSO-d_6, 125 MHz APT): 10.6, 22.5, 63.3, 71.5, 121.9, 122.2, 129.9, 133.1, 135.6, 145.7. Anal. Calcd for $C_{12}H_{14}ClN_3O$: C, 57.26; H 5.61; N, 16.69. Found: C, 57.42; H, 5.82; N, 16.37.

*2.1.1.11. 1-(2,5-dichlorophenyl)-4-(ethoxymethyl)-1H-1,2,3-triazole (**9g**).* Yellow oil, 50% yield; IR (KBr, cm^{-1}): ν 3141, 2975, 2868, 1732, 1588, 1487, 1448, 1376, 1231, 1097, 1038, 874, 809, 698, 671, 651; ^{1}H NMR (DMSO-d_6, 500 MHz): 1.27 (3H, t, *J* 3.9 Hz), 3.67 (2H, q, *J* 3.9 Hz), 4.70 (s, 2H), 7.84 (1H, dd, *J* 1.5 and 5.4 Hz), 7,92 (1H, d, *J* 5.4 Hz), 8.02 (1H, d, *J* 1.5 Hz), 8.63 (1H, s); ^{13}C NMR (DMSO-d_6, 125 MHz APT): 14.9, 62.8, 65.0, 125.8, 127.4, 128.0, 131.2, 131.8, 132.4, 135.5, 144.4. Anal. Calcd for $C_{11}H_{11}Cl_2N_3O$: C, 48.55; H 4.07; N, 15.44. Found: C, 48.63; H, 4.02; N, 15.37.

*2.1.1.12. 1-(2,5-dichlorophenyl)-4-(propoxymethyl)-1H-1,2,3-triazole (**9h**).* Yellow oil, 50% yield; IR (KBr, cm^{-1}): ν 2962, 2872, 1588, 1486, 1450, 1369, 1231, 1096, 1037, 1000, 874, 811, 760, 694, 651; ^{1}H NMR (DMSO-d_6, 500 MHz): 0.99 (3H, t, *J* 7.0 Hz), 1.67 (2H, p, *J* 7.0 Hz), 3.58 (2H, t, *J* 7.0 Hz), 3.61 (2H, t, *J* 6.9 Hz), 4.72 (2H, s), 7.85 (1H, dd, *J* 2.5 and 9.0 Hz), 7.92 (1H, d, *J* 9.0 Hz), 8.01 (1H, d, *J* 3.0 Hz); 8.66 (1H, s); ^{13}C NMR (DMSO-d_6, 125 MHz APT): 10.5, 22.4, 63.0, 71.3, 125.9, 127.5, 128.2, 131.4, 131.9, 132.5, 135.5, 144.4. Anal. Calcd for $C_{12}H_{13}Cl_2N_3O$: C, 50.37; H 4.58; N, 14.68. Found: C, 50.24; H, 4.52; N, 15.30.

*2.1.1.13. 1-(3,5-dichlorophenyl)-4-(ethoxymethyl)-1H-1,2,3-triazole (**9j**).* Yellow solid, 54% yield; m.p. 49-50ºC; IR (KBr, cm^{-1}): ν 2974, 2927, 2865, 1728, 1585, 1475, 1440, 1374, 1334, 1278, 1094, 1039, 851, 807, 666; ^{1}H NMR (DMSO-d_6, 500 MHz): 1.28 (3H, t, *J* 6.5 Hz), 3.67 (2H, t, *J* 6.5 Hz), 4.71 (2H, s), 7.86 (1H, t, *J* 2.0), 8.19 (1H, d, *J* 2.0 Hz), 9.03 (1H, s); ^{13}C NMR (DMSO-d_6, 125 MHz APT): 15.0, 63.0, 65.1, 118.6, 122.4, 127.9, 135.2, 138.3, 145.7. Anal. Calcd for $C_{11}H_{11}Cl_2N_3O$: C, 48.55; H 4.07; N, 15.44. Found: C, 48.66; H, 3.98; N, 15.40.

*2.1.1.14. 1-(3,5-dichlorophenyl)-4-(propoxymethyl)-1H-1,2,3-triazole (**9k**).* Yellow solid, 54% yield; m.p. 49-50ºC; IR (KBr, cm^{-1}): ν 3142, 3048, 2922, 2872, 1585, 1476, 1436, 1365, 1337, 1228, 1088, 1036, 1004, 955, 889, 853, 811, 667; ^{1}H NMR (DMSO-d_6, 500 MHz): 0.88 (3H, t, *J* 7.5 Hz), 1.55 (2H, sex, *J* 7.5 Hz), 3.45 (2H, t, *J* 7.5 Hz), 4.58 (2H, s), 7.74 (2H, t, *J* 2.0 Hz), 8.07 (2H, d, *J* 2.0 Hz), 8.91 (1H, s); ^{13}C NMR (DMSO-d_6, 125 MHz APT): 10.5, 22.4, 63.2, 71.4, 118.5, 122.3, 127.8, 135.2, 138.2, 145.7. Anal. Calcd for $C_{12}H_{13}Cl_2N_3O$: C, 50.37; H 4.58; N, 14.68. Found: C, 50.44; H, 4.59; N, 14.34.

*2.1.1.15. 1-(4-methoxyphenyl)-4-(propoxymethyl)-1H-1,2,3-triazole (**9m**).* Yellow oil, 65% yield; IR (KBr, cm^{-1}): ν 2873, 1611, 1518, 1461, 1377, 1303, 1253, 1190, 1094, 1037, 989, 832, 768, 695; ^{1}H NMR (DMSO-d_6, 500 MHz): 0.99 (3H, t, *J* 7.0 Hz), 1.67 (2H, sex, *J* 7.0 Hz), 3.56 (2H, t, J 7.0 Hz), 3.95 (3H, s), 4.69 (2H, s), 7.23-7.26 (2H, m), 7.90-7.94 (2H, m), 8.78 (1H, s); ^{13}C NMR (DMSO-d_6, 125 MHz APT): 10.5, 22.4, 55.6, 63.3, 71.3, 114.9, 121.7, 122.0, 130.1, 145.1, 159.3. Anal. Calcd for $C_{13}H_{17}N_3O_2$: C, 63.14; H 6.93; N, 16.99. Found: C, 63.44; H, 5.72; N, 16.55.

*2.1.1.16. 4-(butoxymethyl)-1-(4-methoxyphenyl)-1H-1,2,3-triazole (**9n**).* Brown solid, 54% yield; m.p. 63-64ºC; IR (KBr, cm^{-1}): ν 2932, 2866, 1610, 1517, 1462, 1375, 1304, 1254, 1190, 1095, 1039, 989, 831, 767, 695; ^{1}H NMR (DMSO-d_6, 500 MHz): 0.99 (3H, t, *J* 6.9 Hz); 1.41-1.48 (2H, m), 1.60-1.67 (2H, m), 3.60 (2H, t, *J* 6.6 Hz), 3.95 (OCH_3), 4.68 (2H, s), 7.25 (2H, d, *J* 9.2 Hz), 7.92 (2H, d, *J* 9.2 Hz), 8.78 (1H, s); ^{13}C NMR (DMSO-d_6, 125 MHz APT): 13.8, 18.9, 31.2, 55.6, 63.3, 69.4, 114.9, 121.8, 122.0, 130.2, 145.2, 159.3. Anal. Calcd for $C_{14}H_{19}N_3O_2$: C, 64.35; H 7.33; N, 16.08. Found: C, 64.44; H, 6.89; N, 16.35.

*2.1.1.17. 2-phenyl-4-(propoxymethyl)-2H-1,2,3-triazole (**14b**).* Yellow oil, 98% yield; IR (KBr, cm^{-1}): ν 2926, 2873, 1598, 1498, 1462, 1414, 1356, 1312, 1100, 1047, 965, 910, 850, 754, 690, 665; ^{1}H NMR (DMSO-d_6, 500 MHz): 1.00 (3H, t, *J* 7.0 Hz), 1.67 (2H, sex, *J* 7.0 Hz), 3.57 (2H, t, *J* 7.0 Hz), 4.75 (2H, s), 7.51-7.56 (1H, m), 7.66-7.70 (2H, m), 8.10-8.13 (2H, m), 8.18 (1H, s); ^{13}C NMR (DMSO-d_6, 125 MHz APT): 10.5, 22.4, 63.1, 71.6, 118.3, 127.4, 127.6, 135.6, 139.2, 147.3. Anal. Calcd for $C_{12}H_{15}N_3O$: C, 66.34; H, 6.96; N, 19.34. Found: C, 66.49; H, 7.02; N, 19,12.

2.2. Biological Assays

2.2.1. In Vitro experiments

2.2.1.1. Mice peritoneal macrophages. Mice peritoneal macrophages were harvested from male Swiss mice through the lavage of their peritoneal cavity with 10 mL of Dulbecco's modified Eagle's medium (DMEM) medium. Our protocols adhered to the Ethical Principles in Animal Experimentation adopted by the Brazilian College of Animal Experimentation and were approved by the FIOCRUZ Research Ethics Committee (number LW-033/12). The isolated cells were centrifuged and resuspended. Aliquots (0.5 mL) of cell suspension were added to microplate wells and placed in a humidified atmosphere (37 °C, 5% CO_2) for 30 minutes for cell adhesion. Non-adherent cells were removed by washing with DMEM medium containing 10% fetal bovine serum (FBS) and gentamycin (1 μL/mL). Firmly adhering cells were re-suspended in phenol red-free DMEM medium and used for subsequent experimental procedures.

2.2.1.2. HEK-293 cells transfected with P2X7R. HEK-293 cells expressing P2X7R were maintained in DMEM supplemented with 10% fetal bovine serum (FBS), 2 mM L-glutamine, and antibiotics (50 U/ml penicillin and 50 mg/ml streptomycin) in a humidified 5% CO_2 atmosphere at 37 °C. After diluting to 2.5 X 10^6 cells/ml, 80 mL of the cell suspension was added to each well of 96-well culture plates. The **9d** derivative was incubated for 10 minutes and then ATP was added, and the cells were incubated for 20 minutes in a humidified 5% CO2 atmosphere at 37 °C. After incubation, a Gemini fluorescence plate reader was used to measure the absorbance at an excitation wavelength of 530 nm and an emission wavelength of 620 nm. The inhibition (percent) of ethidium ion uptake was expressed as a relative value of the maximum accumulation when stimulated with ATP. To calculate IC_{50} values, we calculated a series of dose-response data using nonlinear regression analysis (i.e., percentage accumulation of ethidium bromide vs compound concentration).

2.2.1.3. Spectrofluorometric Measurement of Dye uptake. Peritoneal macrophages expressing the P2X7Rs were resuspended at 2.5 x 10^6 cells/mL in assay buffer composed of 10 mM HEPES, 5 mM KCl, 1 mM $MgCl_2$, 1 mM $CaCl_2$ and 140 mM NaCl (pH 7.4). The 1,2,3-triazole derivatives or Brilliant Blue G (BBG) (as a standard inhibitor) was added to each sample, followed by the P2X7R agonist ATP or BzATP. The plates were incubated at 37 °C for 30 minutes, and the cellular accumulation of propidium iodide (PI) to peritoneal macrophages assays and ethidium bromide (EB) to HEK-293 trasfected cells was determined by measuring the fluorescence with a Molecular Devices SpectraMax M5 fluorescent plate reader (excitation wavelength 530 nm; emission wavelength 590 nm).

2.2.1.4. LDH Release Assay. The presence of LDH in the media was detected in all of the experiments using a cytotoxicity detection kit (Sigma kit for LDH) according to the manufacturer's instructions. The cell supernatants were tested for LDH, which reduces NAD^+, which in turn converts tetrazolium dye into a soluble, colored formazan derivative. In this assay, we treated the cells for 1 h, 24 h and 72 h with 1,2,3-triazole derivatives.

2.2.1.5. Dye uptake assay. Cell permeabilization was visualized by the differential uptake of propidium iodide (696 Da). Macrophages were incubated with 1 mM ATP or 100 µM BzATP, with or without P2X7R antagonists or 1,2,3-triazole analogs for 25 minutes at 37 °C. PI (0.05 mg/mL in PBS) or ethidium bromide (750 ng/mL in PBS) was added during the last 5 minutes of the incubation. Microplate wells were washed with saline solution (150 mM KCl, 5 mM NaCl, 1 mM $MgCl_2$, 0.1 mM EGTA and 10 mM HEPES, pH 7.4) or PBS, pH 7.4 and observed under a fluorescence microscope (Nikon) equipped with rhodamine (546/FT 580/LP 590) and fluorescein (450-490/FT 510/LP 520) filters. The fluorescence pattern was also analyzed by flow cytometry. Dead cells and cellular debris were excluded based on low forward and side scatters and an extremely high fluorescence profile. Simultaneously, samples with 1 mM ATP, with or without P2X7R antagonists or 1,2,3-triazole analogs were incubated at 37 °C for 25 minutes; the PI was added during the final 5 minutes and the samples were analyzed immediately. The 1,2,3-triazole analog doses varied from 0.01 ng/mL to 10 µg/mL. P2X7R antagonists (BBG or A740003) were used as the control.

2.2.1.6. Electrophysiological measurements. A whole-cell configuration was set up as described by Faria and coworkers [61]. The series resistance was 5-11 MΩ for all of the experiments in standard saline (bath and pipette solutions), and no compensation was applied for currents less than 1500 pA. Above this level, the currents were compensated by 90%. Measurements were discarded when the series resistance was increased substantially. Macrophage (mean ± s.d., 13.2 ± 4.44 pF; n = 106) cell capacitance was measured by applying a 20 mV hyperpolarizing pulse from a holding potential of 20 mV; the capacitive transient was then integrated and divided by the amplitude of the voltage step (20 mV). All recordings were obtained in a holding potential of -60 mV at 37 °C.

2.2.1.7. Saline solutions for electrophysiology. Different saline solutions were used in the pipette or the bath, depending on the protocol. The bath solution (in mM) consisted of the following: 150 NaCl, 5 KCl, 1 $MgCl_2$, 1 $CaCl_2$, and 10 HEPES (pH, 7.4); the pipette solution (in mM) consisted of the following: 150 KCl, 5 NaCl, 1 $MgCl_2$, 10 HEPES, and 0.1 EGTA (pH, 7.4).

2.2.1.8. Drug application. Patch clamp experiments were performed under perfusion (RC-24 chamber, Warner Instrument Corp.) at a rate of 1 mL/min to confirm the data obtained by micropipette application. All of the drugs were dissolved in saline solution immediately before use. Ion currents were studied by applying 1 mM ATP (for 300 s) and adding or not adding 1,2,3-triazole derivatives or BBG.

2.2.1.9. IL-1β production by THP-1 macrophages and mice peritoneal macrophages. THP-1 cells were maintained in Roswell Park Memorial Institute 1640 medium (RPMI medium) supplemented with 10% FBS, penicillin (100 U/ml), and streptomycin (100 mg/ml) in a humidified 5% CO_2 atmosphere at 37 °C. Cells were plated at 2 X 10^5 cells/well in 96-well culture plates, and 500 ng/ml of phorbol 12-myristate 13-acetate (PMA) and 10 ng/ml of IFN-γ were co-treated for 24 h to differentiate human monocytic THP-1 cells into macrophage-like cells. PMA-differentiated human THP-1 macrophages were treated with BBG, A740003 and **9d** derivative for 30 minutes at 37 °C, followed by stimulation with LPS (1 µg/ml) for 4 h. THP- 1 cells received 1 mM ATP for 30 minutes at 37 °C. Cells were centrifuged at 1000 rpm for 5 minutes at 4 °C, and the supernatants were collected and stored at -70 °C. IL-1*β* release was measured using a Human IL-1 beta ELISA Kit (ab46052 -ABCAM, Cambridge).

Peritoneal macrophages were primed 4 hours with LPS 100 ng/mL. After washes with PBS, these macrophages were treated with 1 mM ATP for 30 min at 37 ºC. In some assays, BBG, A740003 and **9d** derivative were added 15 min before the addition of LPS or ATP. The mature form of IL- released from macrophages was quantified by sandwich ELISA following manufacturers' protocols (eBioscience (San Diego, CA, USA).

2.2.1.10. Caco-2 cells culture and incubations. Caco-2 cells were seeded in 96-well polyester Corning® Costar® transwell plates (Sigma-Aldrich, St. Louis, MO, USA) at a density of 3 × 105 cells/well with medium (DMEM with 10% fetal calf serum. Caco-2 cells cultured for up to 21 days in a humidified incubator maintained at 37 °C in an atmosphere of 5% CO_2. The medium and monolayer integrity were checked every 3 days by measuring the Lucifer Yellow. On the day of experiment, working solutions of the **9d**, vinblastine (poor permeability control), and propranolol (high permeability control) at 100 µM were prepared in transport buffer (HBSS and 25 mM HEPES) at pH 7.4 or 6.5 and 0.5% (v/v) DMSO. Cells were washed with prewarmed (37 ºC) transport buffer at the corresponding pH. To equilibrate the cells with the transport buffer, 0.3 mL of transport buffer were added to the wells. Feeder tray was substituted for a 24- well Enhanced

Recovery Plate with 1 mL of transport buffer at pH 7.4. These plates are treated with a hydrophilic covalent coating to resist nonspecific adsorption of compounds. Then, cells were incubated for 30 minutes at 37 °C and 5% CO_2. After this time, transport buffer in the apical wells was removed and 0.3 mL of the corresponding **9d**, vinblastine or propranolol solution was added. The cells were placed again in the incubator for 60 minutes. Then the plates were separated, and LY concentrations were measured in the donor and acceptor wells and initial solution. For lucifer yellow, fluorescence was measured at plate reader M5 (molecular probes) at excitation 485 nm and emission 530 nm.

*2.2.1.11. pH Dependent Solubility of **9d***. Kinetic solubility **9d** was assessed from 1 to 250 µM by spiking DMSO stock solutions (5 µL, in triplicate) into 995 µL buffer (pH 2.0-hydrochloride, 4.0-100 mM citrate buffer and 7.4-100 mM phosphate buffer) in a 96-well plate and placing at room temperature for 2 h. Calibration standards were constructed by spiking 5 µL of DMSO stock solutions into 995 µL acetonitrile/buffer (1:1) mixture. After centrifugation (10,000 rpm, 10 min, 25 ºC) the reaction samples were diluted 1:1 with acetonitrile.

2.2.1.12. Distribution coefficient (Log D) in octanol/PBS pH 7.4. Octanol and PBS pH 7.4 with ratio 1:1 (v/v) taken in a flask and shaken mechanically for 24 hours to pre-saturate PBS with octanol and octanol with PBS. Pre-saturated solvents were used for the present study in according to [62] methodogy. Triazole **9d** in a volume of 4 µL and concentration of 25 mM added in 396 µL PBS undergo partitioning with different volumes of octanol (100- 400 µl). After 2 hours with vigorous shaking for mixture, centrifugation at 3000 rpm for 5 minutes to separate, followed by 1 hour standing without disturbance. PBS layer was taken out. Acetonitrile (100 µl) added to a 100 µl PBS aliquot had its absorbance measured (396 µL PBS containing 4 µL of 25 mM **9d** + 400 µL acetonitrile). Two standard compounds were similarly studied to validate the assay.

2.2.1.13. In vitro stability assays in liver microsomes. Liver microsomes from male mouse and human with final protein concentration of 0.5 mg/ml in 0.1 M phosphate buffer at pH 7.4. Triazole **9d** with final concentration of 1 µM and DMSO concentration of 0.5 µM were pre-incubated at 37 °C before NADPH addition with final concentration of 1mM to initiate the reaction. The final incubation volume was 50 µl. Buffer containing 0.1 M phosphate at pH7.4 was used as control replacing NADPH (minus NADPH). Diazepam for mice , and verapamil for human were incubated as positive control. Triazole **9d** and controls were incubated for 0, 5, 15, 30 and 45 min. Negative control (minus NADPH) was incubated for 45 min. only. Methanol (50 µL) was used to stop

reactions at the appropriate time points. Samples incubated in plates were centrifuged at 1640 × g for 20 min. at 4 °C to aid protein precipitation.

In vitro intrinsic clearance (CLint mic) for the metabolism of **9d** in mouse and human liver microsomes was calculated using equations below:

Half life ($t_{1/2}$) (min) = 0.693/k (1)

V(µL/mg) = volume of incubation (µL)/protein in the incubation (mg) (2)

Intrinsic Clearance (CL_{int}) (µL/min/ mg protein) = V x 0.693/ t1/2 (3)

in according to Biosystem instructions.

2.2.2. In Vivo experiments

Male *Swiss Webster* mice (18 to 20 g) provided by Oswaldo Cruz Foundation breeding unit (Fiocruz, Rio de Janeiro, Brazil) were used. Mice were caged with free access to food and fresh water in a room with temperature ranging from 22 to 24 °C and a 12 h light/dark cycle at Helio & Peggy Pereira vivarium experimental animal facility. All experimental procedures were performed according to Oswaldo Cruz Foundation's Committee on Ethical Use of Laboratory Animals (number LW-58/14).

2.2.2.1. Paw edema. The *in vivo* efficacy of the novel P2X7R antagonists in the 1,2,3-triazole series was evaluated using a paw edema inflammatory model. In these experiments, 1,2,3-triazole were administered oral (for gavage) or intraperitoneally 60 minutes prior to the intrathecal administration of a 1 mM ATP saline suspension. Thirty minutes later, the paw edema was measured and the animals were euthanized by CO_2 inhalation, and their peritoneal cavities were lavaged (2 x 15 mL) with ice-cold phosphate-buffered saline (w/o Ca^{2+} and Mg^{2+}). For cytokine determinations, the samples were spun at 10000 X g in a refrigerated microfuge (4 °C). The supernatants were removed and frozen until the IL-1β levels were determined by ELISA technique.

2.2.2.2. LPS-induced pleurisy. Male Swiss mice received intrathoracic (i.t.) injection of 0.1 mL of LPS (250 ng/cavity, from *E. coli* serotype 0127:B8) or vehicle (control group) using an adapted needle (13 x 0.45 mm) carefully inserted at a depth of 1 mm into the right side of the thoracic cavity of mice. Twenty four hours after the stimulus, the animals were killed in a CO_2 chamber, the

thoracic cavity was opened and washed with 1 mL of heparinized saline (10 UI ml^{-1}). Pleural wash aliquots were collected and diluted in Turk solution (2% acetic acid) for total leucocyte count in Neubauer chambers. Differential leucocyte analysis was performed on cytocentrifuged smears stained by the May-Grunwald-Giemsa method Sterile saline (0.9%)-injected animals constituted the control group.

2.2.2.3. Leukocyte counts. Total leukocyte counts were made in Neubauer chamber, under an optical microscope, after dilution in Türk fluid (2% acetic acid). Differential counts of mononuclear cells, neutrophils and eosinophils were made by using stained cytospins (Cytospin 3, Shandon Inc., Pittsburgh, PA) by May-Grünwald-Giemsa method. Counts are reported as numbers of cells per cavity.

2.2.2.4. Statistical analyses. Statistical comparisons were expressed as the mean ± SD (standard deviation) as indicated in the text. The statistical significance of the differences between means was tested by one-way ANOVA followed by Tukey's test. A bicaudal $p < 0.05$ was considered significant.

2.3. In Silico evaluation

2.3.1. ADMET properties. The prediction of the compounds druglikness such as pharmacokinetic and toxicological profile are important parameters for drug design. Thus, the screening of the compound **9d** toxicity profile was performed using Osiris® program from Actelion Pharmaceuticals Ltda. (http://www.organic-chemistry.org/prog/peo/) and the compound **9d** pharmacokinetic profile was performed by ADMET Predictor® (Simulation Plus).

2.3.2. Ligand preparation. The inhibitors (**9d, 8h** and **12**) molecular structure was built by Spartan´10 v.1.0.1. Thus, the conformer distribution was applied to obtain the local energy minimum conformers using MMFF force field [63]. A selected conformer was submitted to equilibrium geometry applying the RM1 (Recife Model 1) semi-empirical method [64]. Finally, the single point energy calculation was performed by the Density Function Theory (DFT) using B3LYP/6-31G** quantum basis sets [65-67].

2.3.3. Molecular docking. The molecular docking was carried out by AutoDock Vina program [68,69]. For this purpose the apo closed state human trimeric protein P2X7 structure was retrieved

from the Protein Data Bank (PDB ID: 5U1L) [70]. Both receptor and ligand were previously prepared by AutoDock tools 4.2.6 which included the addition of hydrogen atoms as well as Gasteiger charges. The grid box of dimension 16x16x16 Å was centered around the eight conserved residues known to be involved in ATP binding cavity such as: Lys64, Lys66, Phe188 and Thr189 from one subunit, and Asn292, Phe293, Arg294 and Lys311 from an adjacent subunit [71,72]. For supporting this docking approach a re-docking was performed by using the crystal complex P2X7-JNJ47965567 recently deposited in the Protein Data Bank by the code 5U1X. The re-docking clearly identifies that the ligand JNJ47965567 docked preferably in the allosteric site, which comprises a groove formed between two neighboring subunits. In addition, a further re-docking centered on the allosteric site reproduced the main interaction performed by the ligand in the crystal structure. The superposition of the ligand JNJ47965567 crystal structure and conformation generated by the re-docking is presented in Fig. 1.

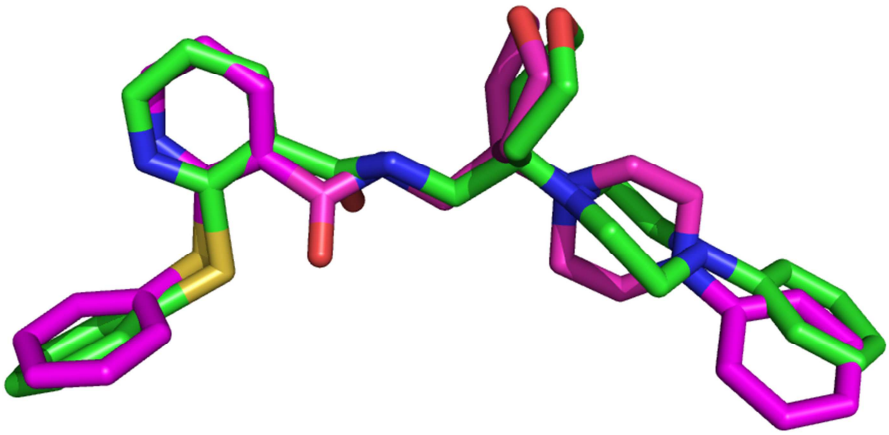

Fig. 1. superposition of the ligand JNJ47965567 into the crystal P2X7 structure (PDB ID: 5U1X). In green is depcted the crystal binding pose and in pink is depicted the best docking obtained from AutoDock Vina program

3. Results

3.1. Chemistry

3.1.1. Synthesis of 1H -1,2,3-triazoles [73]

The method used to prepare the 1*H*-1,2,3-triazole was based on a variant of the Huisgen 1,3-dipolar cycloaddition protocol [74] in which a reaction of aryl azides (from anilines **1a-e**) and propargylic alcohol was catalyzed by Cu(I), providing only regioisomer 1,4-disubstituted **5a-e** at high yields (55-82%). The partial oxidation of **5** generated the 4-carboxaldehyde-1*H*-1,2,3-triazoles (**6a-c**) with yields ranging from 64-84%, and afterwards, treating with $NH_2OH{\cdot}HCl$ in caustic solution yielded oximes (**7a,b**). The esterified (**8a-q**) and etherified (**9a-n**) derivatives were made from a nucleophilic substitution reaction between the alcohol (**5**) and acid chlorides or alkyl bromides in basic medium, respectively (Fig. 2).

The 2*H*-1,2,3-triazole series was obtained starting from Fischer's method to obtain glucoseosazone **3** from D-glucose, followed by oxidative cyclization by Hudson's method (refluxing in an aqueous solution of $CuSO_4$). This method generated the osotriazole **4**, which by treatment with aqueous $NaIO_4$ afforded the 3-carboxaldehyde-2*H*-1,2,3-triazoles (**10**). In sequence, we synthesized 2*H*-1,2,3-triazole alcohol (**12**) by reduction with $NaBH_4$, which was obtained at a quantitative yield. The oxime (**11**), the esters (**13a-d**) and the ethers (**14a-c**) were prepared using the same protocol as above with yields ranging from 30% to quantitative (Fig. 2).

1*H*-1,2,3-Triazole Series

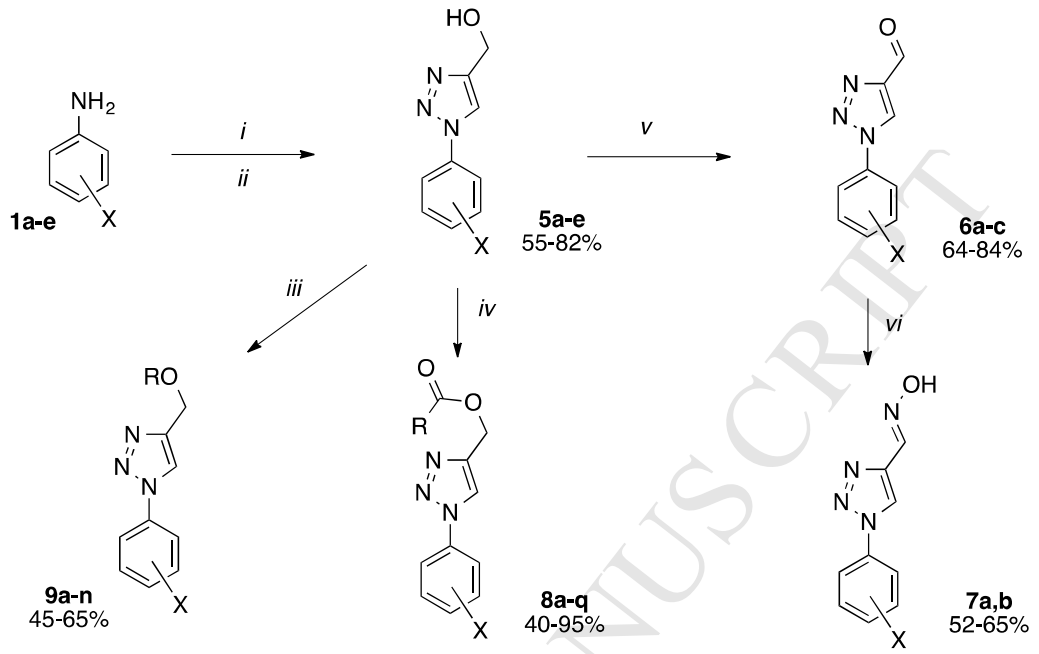

2*H*-1,2,3-Triazole Series

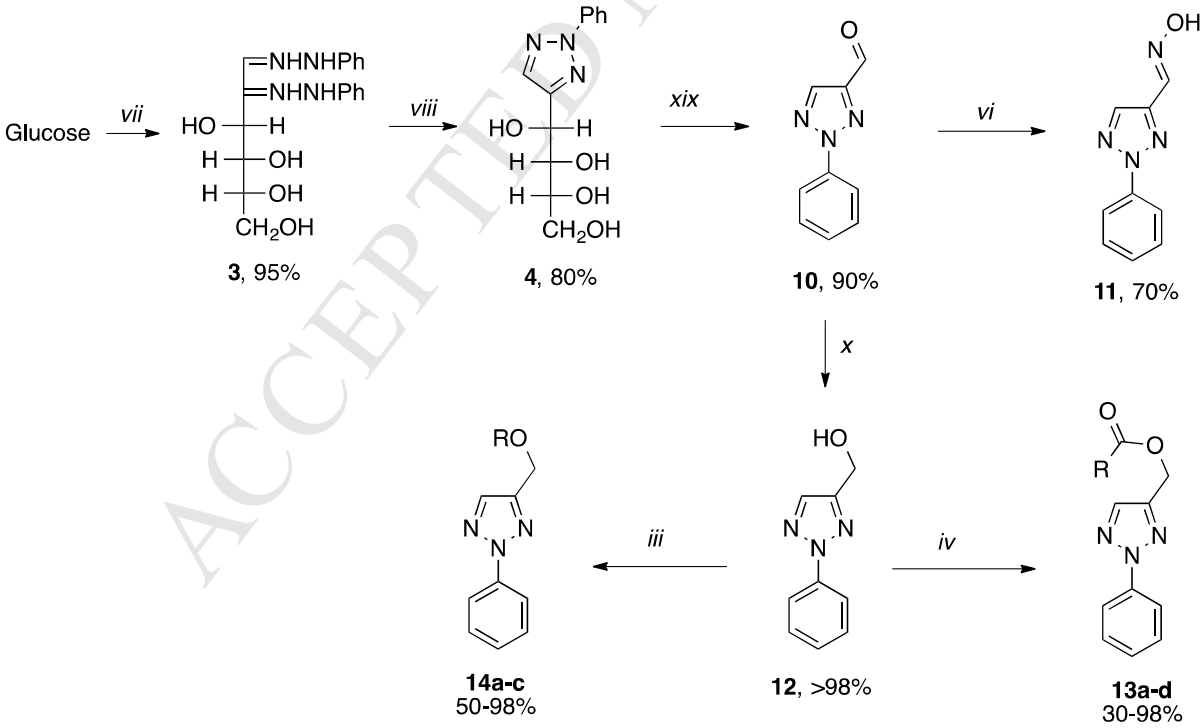

Fig. 2. Synthetic routes to 1*H*-1,2,3- and 2*H*-1,2,3-triazole series. The reagents and conditions were as follows: i) $NaNO_2$, $HCl_{(aq)}$ 50%, 0-5 ºC then NaN_3, H_2O; ii) Propargylic alcohol, $CuSO_4$, ascorbic acid, *t*BuOH, H_2O; iii) R-Br, THF, NaH, reflux; iv) RCOCl, CH_2Cl_2, Pyridine, DMAP, rt; v) IBX,

DMSO, rt; vi) $NH_2OH.HCl$, CH_2Cl_2, Pyridine, rt; vii) $PhNHNH_2.HCl$, H_2O, reflux; viii) $CuSO_4$, H_2O, reflux; xix) $NaIO_4$, H_2O, rt and x) $NaBH_4$, CH_3OH, rt.

3.2. Biology

3.2.1. In Vitro

P2X7R function was measured using whole cell experiments and dye uptake assays in mice peritoneal macrophages (MPM) and HEK 293 cell transfected with hP2X7R.

Triazoles screning activity against mice P2X7R functionality. ATP-induced pore formation in MPM measure with a Fluorescent Imaging Plate Reader (FLIPR). We screened the antagonistic 1,2,3-triazole analogs inhibitory activity using 10 μM as cutoff. MPM in 96-well plates were treated with 10 μM 1,2,3-triazole analogs in the presence of 1 mM ATP for 15 minutes. We grouped compounds according to their chemical groups to facilitate the understanding of the results. In parallel, we measured LDH release induced by 1,2,3-triazoles alone in the concentration of 10 μM after 60 minutes of continuous exposition. As criterions to select the promising triazoles, we considered the compounds with percentage inhibition higher than 75%, when compared to ATP response alone and toxicity less than 20%.

As shown in Table 1, when we applied esters triazoles in MPM, the molecules **8f**, **8g**, **8i**, **8k**, **8l**, **8m**, **8n**, and **8q** did not block ATP-induced dye uptake. Analogues **8a**, **8c**, **8p**, **13c** and **13d** modestly inhibited ATP-induced dye uptake. Analogues **8b**, **8d**, **8e**, **8h, 8j, 13a** and **13b** inhibited P2X7R pore formation in comparison with treatments with 1 mM ATP alone. When we studied the toxicity caused by these compounds (Table 1), triazoles **8a**, **8b**, **8d**, **8e**, **8g**, **8i**, **8j**, **8k**, **8m**, **8n**, **8q**, **13a, 13b, 13c** and **13d** released more than 20% of LDH, and they were considered toxic in comparison with the negative control. Among the esters compounds, analog **8j** inhibited ATP-induced pore formation in a manner similar to that of BBG (Table 1), but it exhibited considerable toxicity relative to the negative control (Table 1, compare the second with fourth column). Merely, ester containing compound **8h** inhibited ATP-induced dye uptake and showed low toxicity to mammalian cells.

Table 1. Effects of ester triazoles in P2X7R antagonistic activity

Compound	% Inhibition (a)	% LDH release (b)
8a (X = H, R = Ph)	32.1 ± 2.02	58.1 ± 4.86
8b (X = H, R = Me)	83.95 ± 2.93	36.39 ± 11.02

8c (X = H, R = pentyl)	44.6 ± 0.46	15.83 ± 1.3
8d (X = H, R = nonyl)	59.99 ± 8.34	42.53 ± 0.4
8e (X = 4-Cl, R = Ph)	60.61 ± 5.78	45.73 ± 1.71
8f (X = 4-Cl, R = Me)	23.18 ± 6.75	19.66 ± 0.6
8g (X = 4-Cl, R = pentyl)	11.1 ± 4.52	34.19 ± 2.01
8h (X = 4-Cl, R = nonyl)	76 ± 2.9	8 ± 0.6
8i (X = 2,5-diCl, R = Ph)	11 ± 10.44	26.66 ± 1.2
8j (X = 2,5-diCl, R = Me)	76.6 ± 2.95	32 ± 1
8k (X = 2,5-diCl, R = pentyl)	20.65 ± 8.26	22.66 ± 0.3
8l (X = 2,5-diCl, R = nonyl)	9.86 ± 4.87	10 ± 0.7
8m (X = 3,5-diCl, R = Ph)	14.21 ± 4.83	24.02 ± 1.7
8n (X = 3,5-diCl, R = Me)	65.18 ± 1.88	45.33 ± 1.4
8o (X = 4-OMe, R = Ph)	24.38 ± 3.94	10.66 ± 0.5
8p (X = 4-OMe, R = Me)	29.44 ± 2.99	15 ± 1.9
8q (X = 4-OMe, R = pentyl)	26.55 ± 4.22	46.3 ± 5.12
13a (R = Ph)	81.3 ± 2.91	36.94 ± 10.6
13b (R = Me)	73.5 ± 1.95	38.5 ± 6.2
13c (R = pentyl)	29.6 ± 0.37	43.04 ± 5.01
13d (R = nonyl)	29.5 ± 4.02	42.5 ± 1.04
BBG (c)	78.89 ± 3.81	13.22 ± 2.66

(a) % Inhibition values at 10 µM were expressed as a percentage, relative to maximum uptake of propidium stimulated by 1 mM ATP only. Data values are expressed as means ± SDs. All experiments were repeated at least 3 and 5 times.

(b) % LDH release values at 10 µM were expressed as a percentage, relative to maximum LDH release caused by 0.05% Triton X- 100 only. Data values are expressed as means ± SDs. All experiments were repeated at least 3 and 4 times.

(c) BBG concentration of 750 nM.

Alcohol containing triazoles derivatives **5a-d** did not diminish ATP-induced dye uptake (Table 2), however compounds **5e** and **12** led to inhibition with low cytotoxic. For this reason, we ruled out **5a**, **5b**, **5c** and **5d** triazoles.

Four synthesized aldehydes are shown in the Table 2. Analogs **6b** and **10** alone were not able to inhibit ATP-induced pore formation. Other analogs, namely **6a** and **6c,** impaired ATP-induced dye uptake. They showed low cytotoxic when applied for 60 minutes. Additionally, compound **6a** effectively diminished ATP-induced dye uptake compared with ATP treatment alone and **6c** partially reduced.

Table 2. Effects of alcohol, aldehyde and oxime triazoles in P2X7R antagonistic activity

	Compound	**% Inhibition (a)**	**% LDH release (b)**
Alcohol	**5a (X = H)**	10.87 ± 3.96	20.98 ± 0.2
	5b (X = 4-Cl)	22.52 ± 1.86	15.57 ± 3.2
	5c (X = 2,5-diCl)	28.33 ± 1.7	12.09 ± 0.01
	5d (X = 3,5-diCl)	11.36 ± 1.89	30.55 ± 5.81

	5e (X = 4-OMe)	86.31 ± 1.03	9.7 ± 2.1
	12	84.16 ± 1.91	9.18 ± 0.4
Aldehyde	**6a (X = H)**	84.6 ± 1.19	10.51 ± 0.82
	6b (X = 2,5-diCl)	36.74 ± 1.21	13.73 ± 0.72
	6c (X = 4-OMe)	44.26 ± 7.33	17.92 ± 6.61
	10	31.49 ± 1.98	41.65 ± 1.62
Oxime	**7a (X = H)**	57.99 ± 0.86	28.59 ± 0.5
	7b (X = 3,5-diCl)	57.99 ± 6.39	29.47 ± 0.7
	11	83 ± 0.58	12.66 ± 0.2
	BBG (c)	78.89 ± 3.81	13.22 ± 2.66

(a) % Inhibition values at 10 µM were expressed as a percentage, relative to maximum uptake of propidium stimulated by 1mM ATP only. Data values are expressed as means ± SDs. All experiments were repeated at least 3 and 5 times.

(b) % LDH release values at 10 µM were expressed as a percentage, relative to maximum LDH release caused by 0.05% Triton X- 100 only. Data values are expressed as means ± SDs. All experiments were repeated at least 3 and 4 times.

(c) BBG concentration of 750 nM.

As shown in Table 2, we evaluated oximes **7a**, **7b** and **11**. Three oximes **7a**, **7b** and **11** inhibited the ATP-induced pore formation. However, compounds **7a** and **7b** had a discreet cytotoxicity (Table 2). Only analog **11** diminished ATP-induced dye uptake, and it did not exhibit toxicity (Table 2).

Ether triazole effects were tested on ATP-induced dye uptake. **9b**, **9h**, **9k, 9m** and **14b** triazoles did not inhibit ATP- induced dye uptake (Table 3). Analogs **9a**, **9e**, **9f**, **9j**, **9l**, **9n**, **14a** and **14c** partially inhibited ATP-induced uptake, and all of them exhibited modest cytotoxicity (Table 3). Conversely, analogs **9c**, **9d**, **9g**, and **9i** effectively blocked the ATP action via P2X7R activation (Table 3). However, **9c** and **9g** displayed cytotoxicity against MPM. Analogs **9d** and **9i** showed low toxic and blocked ATP-induced pore formation (Table 3).

Table 3. Effects of ether triazoles in P2X7R antagonistic activity

Compound	% Inhibition (a)	% LDH release (b)
9a (X = H, R = Et)	49.30 ± 0.82	52.73 ± 0.87
9b (X = H, R = Pr)	25.14 ± 1.01	14.66 ± 0.32
9c (X = H, R = Bu)	78.1 ± 0.71	32.33 ± 1.1
9d (X = 4-Cl, R = Et)	84.67 ± 0.65	8.33 ± 0.2
9e (X = 4-Cl, R = Pr)	32.47 ± 6.22	26.66 ± 1.16
9f (X = 4-Cl, R = Bu)	35.78 ± 0.43	30.33 ± 0.99
9g (X = 2,5-diCl, R = Et)	75.5 ± 1.11	42.66 ± 0.68
9h (X = 2,5-diCl, R = Pr)	24.03 ± 8.03	22.66 ± 0.37

9i (X = 2,5-diCl, R = Bu)	79.75 ± 2.61	11.66 ± 0.57
9j (X = 3,5-diCl, R = Et)	36.53 ± 1	34 ± 1.04
9k (X = 3,5-diCl, R = Pr)	23.96 ± 1.3	14.03 ± 0.41
9l (X = 4-OMe, R = Et)	44.79 ± 7.04	20.66 ± 4.98
9m (X = 4-OMe, R = Pr)	15.62 ± 2.55	13.03 ± 0.21
9n (X = 4-OMe, R = Bu)	31.38 ± 5.06	27.66 ± 0.14
14a (R = Et)	69.97 ± 0.91	26.49 ± 0.1
14b (R = Pr)	26.61 ± 8.76	13.33 ± 0.1
14c (R = Bu)	37.06 ± 0.33	27.19 ± 0.19
BBG (c)	78.89 ± 3.81	13.22 ± 2.66

(a) % Inhibition values at 10 µM were expressed as a percentage, relative to maximum uptake of propidium stimulated by 1mM ATP only. Data values are expressed as means ± SDs. All experiments were repeated at least 3 and 5 times.

(b) % LDH release values at 10 µM were expressed as a percentage, relative to maximum LDH release caused by 0.05% Triton X- 100 only. Data values are expressed as means ± SDs. All experiments were repeated at least 3 and 4 times.

(c) BBG concentration of 750 nM.

HEK 293 cells transfected with hP2X7R demonstrated an inhibitory profile similar to MPM using FLIPR methodology. Basically, **5e**, **6a**, **8h**, **9d**, **9i**, **11**, and **12** also inhibited ethidium iodide uptake in higher antagonistic activity when compared with other molecules (Tables 4-6).

As observed for MPM, **8b**, **8h**, **8j**, **13a**, and **13b** inhibited hP2X7R. Not all other ester triazoles inhibited ATP-induced ethidium uptake with percentage higher than 75% (Table 4). However, among ester triazoles with inhibitory action against hP2X7R, **8h** was unique no cytotoxicity. **8b**, **8j**, **13a** and **13b** promoted LDH release higher than 20% after 60 minutes of exposition (data not shown). Thus, we selected **8h** to proceed in IC_{50} determination.

Table 4. Effects of ester triazoles in HEK 293 transfected hP2X7R antagonistic activity.

Compound	% Inhibition (a)
8a (X = H, R = Ph)	16,1 ± 1,33
8b (X = H, R = Me)	81,02 ± 4,02
8c (X = H, R = pentyl)	18,2 ± 1,32
8d (X = H, R = nonyl)	23,19 ± 2,02
8e (X = 4-Cl, R = Ph)	26,77 ± 1,99
8f (X = 4-Cl, R = Me)	9,89 ± 2,97
8g (X = 4-Cl, R = pentyl)	2,2 ± 0,97
8h (X = 4-Cl, R = nonyl)	78 ± 3,2
8i (X = 2,5-diCl, R = Ph)	3 ± 1,08
8j (X = 2,5-diCl, R = Me)	71,2 ± 5,41
8k (X = 2,5-diCl, R = pentyl)	7,28 ± 2,05
8l (X = 2,5-diCl, R = nonyl)	1,17 ± 0,32
8m (X = 3,5-diCl, R = Ph)	2,96 ± 0,92
8n (X = 3,5-diCl, R = Me)	29,44 ± 0,9

8o (X = 4-OMe, R = Ph)	10,55 ± 1,01
8p (X = 4-OMe, R = Me)	9,12 ± 1,03
8q (X = 4-OMe, R = pentyl)	8,15 ± 2,01
13a (R = Ph)	88,21 ± 5,78
13b (R = Me)	80,1 ± 6,02
13c (R = pentyl)	10,2 ± 2,99
13d (R = nonyl)	19,16 ± 3,11
BBG (b)	90,08 ± 9,94

(a) % Inhibition values at 10 µM were expressed as a percentage, relative to maximum uptake of ethidium bromide stimulated by 1mM ATP only. Data values are expressed as means ± SDs. All experiments were repeated at least 3 and 5 times.

Regarding to alcohol (**5e**, **12**), aldehyde (**6a**), and oxime (**11**) triazoles, they inhibited hP2X7R, in a similar manner to mP2X7R (Table 5). Not all other alcohol, aldehyde and oximes tested inhibited hP2X7R as observed for mP2X7R.

Table 5. Effects of alcohol, aldehyde and oxime triazoles in HEK 293 transfected hP2X7R antagonistic activity.

Compound	**% Inhibition (a)**
BBG (b)	90,08 ± 9,94
Alcohol	
5a (X = H)	30,13 ± 1,04
5b (X = 4-Cl)	26,13 ± 2,09
5c (X = 2,5-diCl)	38,11 ± 3,04
5d (X = 3,5-diCl)	41,09 ± 3,79
5e (X = 4-OMe)	94,12 ± 2,05
12	90,22 ± 2,77
Aldehyde	
6a (X = H)	95,3 ± 2,87
6b (X = 2,5-diCl)	44,02 ± 5,71
6c (X = 4-OMe)	50,28 ± 4,06
10	42,12 ± 6,08
Oxime	
7a (X = H)	64,3 ± 1,92
7b (X = 3,5-diCl)	62,11 ± 5,02
11	94,3 ± 1,03

(a) % Inhibition values at 10 µM were expressed as a percentage, relative to maximum uptake of ethidium stimulated by 1mM ATP only, Data values are expressed as means ± SDs. All experiments were repeated at least 3 and 5 times.

(b) BBG concentration of 750 nM.

Ether triazoles also showed inhibitory profile similar to mP2X7R, because **9c**, **9d**, and **14a** reduced ATP-induced dye uptake above 75% in comparison to ATP alone. Other ether triazoles did not inhibit or they acted partially (Table 6).

Table 6. Effects of ether triazoles in HEK 293 transfected hP2X7R antagonistic activity.

Compound	% Inhibition (a)
9a (X = H, R = Et)	56,73 ± 5,35
9b (X = H, R = Pr)	20,08 ± 3,6
9c (X = H, R = Bu)	67,52 ± 2,84
9d (X = 4-Cl, R = Et)	96,87 ± 0,22
9e (X = 4-Cl, R = Pr)	62,37 ± 4,41
9f (X = 4-Cl, R = Bu)	15,08 ± 2,02
9g (X = 2,5-diCl, R = Et)	45,3 ± 6,02
9h (X = 2,5-diCl, R = Pr)	46,61 ± 3,13
9i (X = 2,5-diCl, R = Bu)	90,07 ± 0,99
9j (X = 3,5-diCl, R = Et)	51,22 ± 4,7
9k (X = 3,5-diCl, R = Pr)	33,66 ± 3,9
9l (X = 4-OMe, R = Et)	45,02 ± 3,13
9m (X = 4-OMe, R = Pr)	35,77 ± 3,82
9n (X = 4-OMe, R = Bu)	51,29 ± 1,79
14a (R = Et)	79,08 ± 3,44
14b (R = Pr)	41,19 ± 7,03
14c (R = Bu)	16,11 ± 1,09
BBG (b)	90,08 ± 9,94

(a) % Inhibition values at 10 µM were expressed as a percentage, relative to maximum uptake of ethidium stimulated by 1mM ATP only, Data values are expressed as means ± SDs. All experiments were repeated at least 3 and 5 times.

(b) BBG concentration of 750 nM.

After the screening phase, we selected triazoles **5e**, **6a**, **8h**, **9d**, **9i**, **11**, and **12** to investigate their potential as P2X7R antagonists in more detail. As indicated in Fig. 3, we performed dye uptake experiments using flow cytometry to obtain inhibition curves for the selected analogs. ATP treatment increased dye uptake 4 times in comparison with negative control (compare Fig.s 3A1 with 3A2). ATP-induced dye uptake was inhibited after pretreating with BBG (Fig. 3A3), and fluorescence was restored to basal levels. All 1,2,3-triazole analogs (Fig.s 3A4 - 3A10) reduced the ATP effect in a dose-dependent manner (Fig. 3B). The IC_{50} values obtained through the dose-response experiment were 488.4 nM for analog **5e**, 167.4 nM for analog **6a**, 106.8 nM for analog **8h**, 83.40 nM for analog **9d**, 316.9 nM for analog **9i**, 349.2 nM for analog **11** and 95.96 nM for analog **12** (Table 7). In comparison with BBG (which has an IC_{50} value of 110.3 nM), analogs **6a**,

9d, **8h** and **12** were more potent and effective at inhibiting ATP-induced dye uptake. Analogues **5e**, **9i** and **11** displayed potency similar or lower than BBG (Table 7).

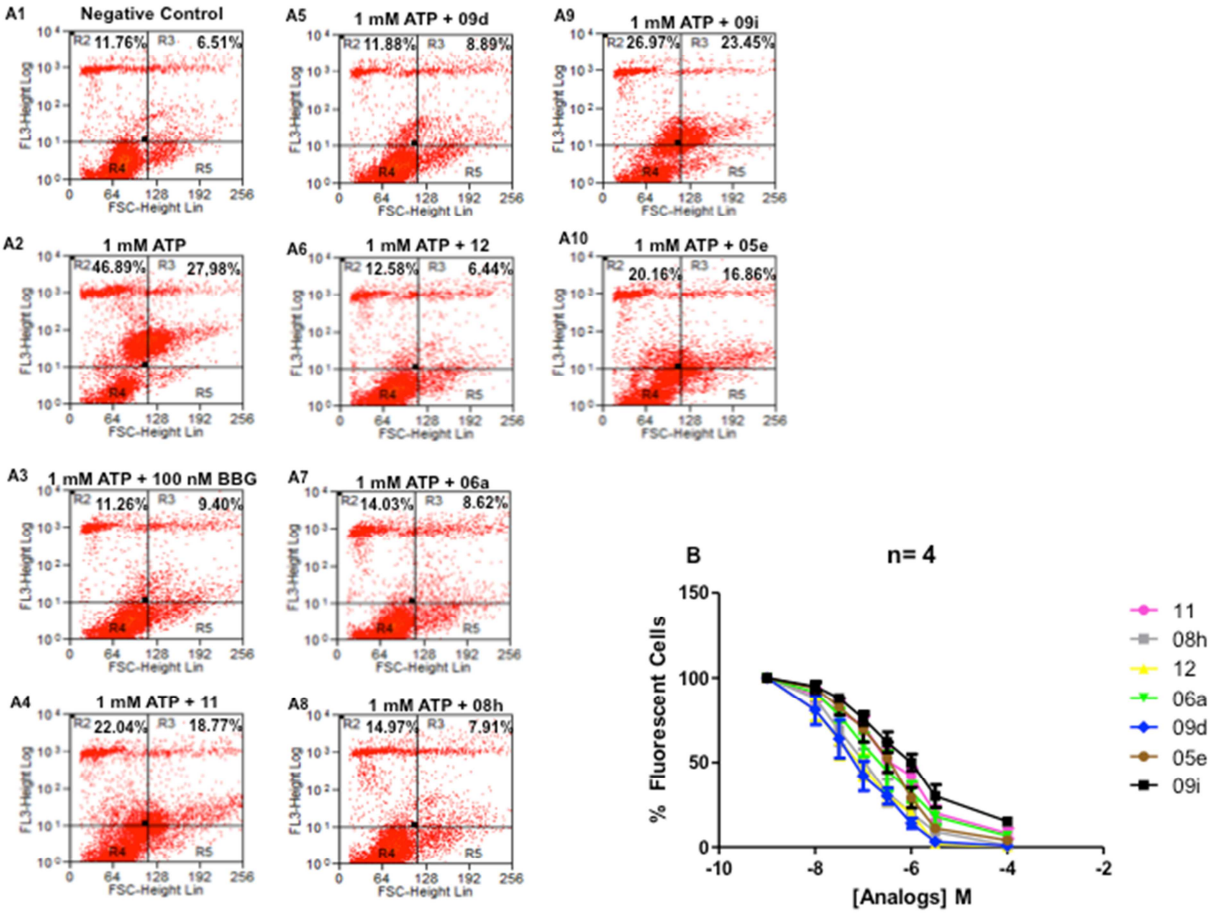

Fig. 3. Dose-concentration inhibition curves for selected 1,2,3-triazole derivatives on pore formation activity. (A) The dot plots are related to ATP-induced dye uptake alone or in the presence of the selected 1,2,3-triazole derivatives. (B) The dose response curves of selected 1,2,3-triazole derivatives with 1 mM ATP for 25 min. as analyzed by flow cytometry to detect the PI uptake. Values represent the mean ± SEM. The profiles are representative of 3-6 independent experiments.

Table 7. Antagonistic effect of triazoles in mice P2X7R.

P2X7R antagonists and Triazoles	*IC_{50} (µM)
BBG	**0.343**
5e	0.488
6a	0.167
8h	0.107
9d	0.083
9i	0.317

11	0.349
12	0.096

*IC_{50} values were obtained from flow cytometry in propidium uptake assay. Data values are expressed as means ± SDs. All experiments were repeated at least 3 times.

Whole cell patch clamp used to study mP2X7R pore macroscopic ionic current evoked after treating with ATP (1 mM ATP) for 5 minutes (black bar), with or without BBG or 1,2,3-triazole analogs (gray bar) in both cases (Fig. 4). ATP-induced ionic currents is represented for Fig. 4A1. BBG reduced ATP-induced current as exhibited at Fig. 4A2. All 1,2,3-triazole analogs diminished ATP-induced macroscopic currents (Fig.s 4A3-4A9). In comparison with BBG, analogs **11**, **5e** and **9i** demonstrated inferior inhibition profile (Fig. 4A7-A9). By contrast, analogs **6a**, **8h**, **9d** and **12** showed an inhibition superior to that of BBG (Fig. 4A3-6). Dose-response curves for selected triazoles and BBG confirms this inhibitory profile (Fig. 4B). As demonstrated in the Table 8, **6a**, **8h**, **9d** and **12** were more potent than BBG to inhibit P2X7R expressed in MPM**.** Analogs **6a** and **8h** obtained a performance similar to BBG. In the other hand, BBG exhibited a higher potency than **05e**, **9i** and **11** (Table 8).

Our results indicate that these four compounds could be promising P2X7R antagonists. All of them inhibited P2X7R at IC_{50} values that were lower than classical P2X7R antagonists, namely suramin, PPADS, KN-62 and oxidized ATP [75,76], and similar to novel antagonists such as A740003, A438079, A804598, AZ10606120, and AZ11645373 [77].

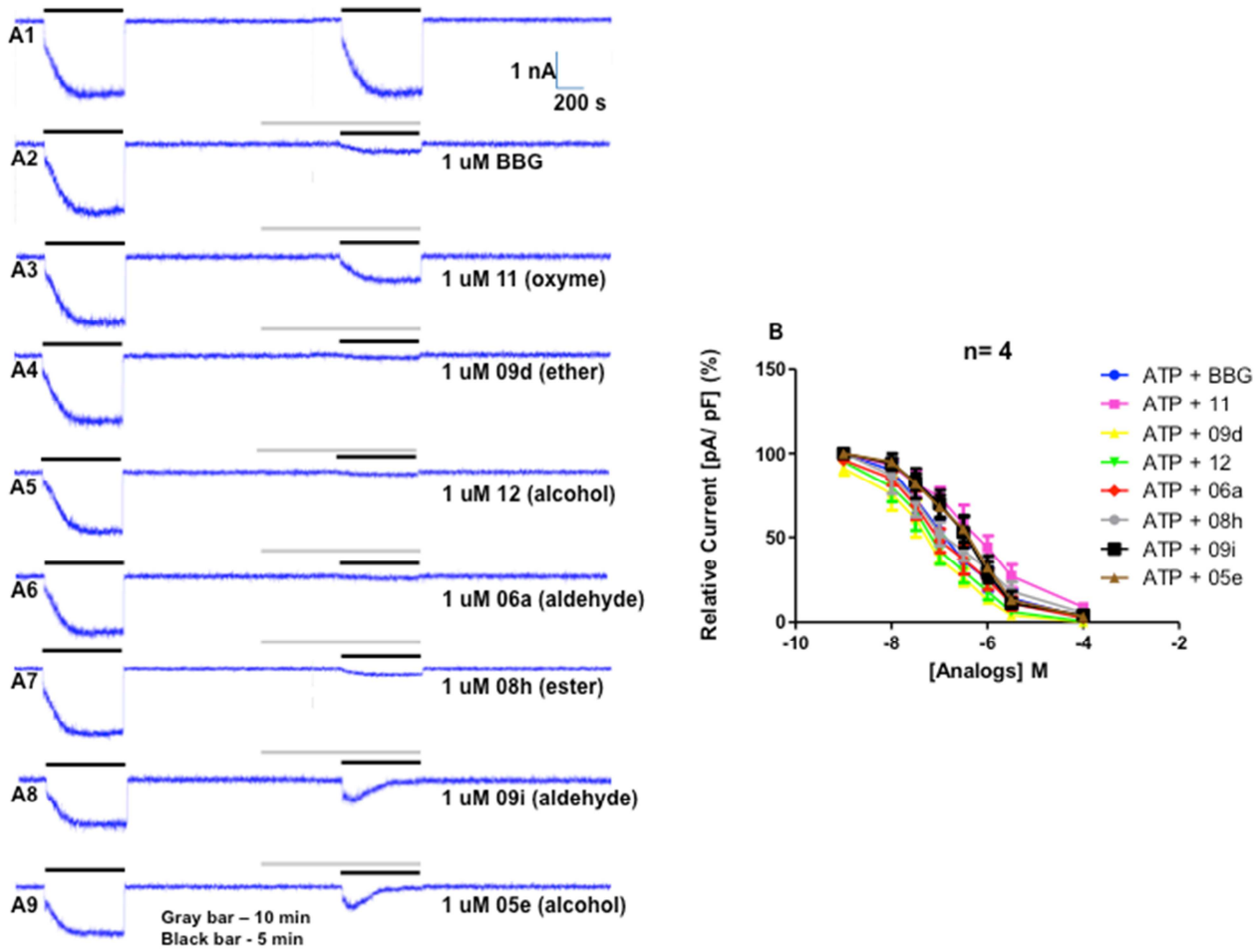

Fig. 4. Macroscopic current induced by ATP is inhibited by selected 1,2,3-triazole derivatives. (A) Whole cell recordings of the cationic P2X7R activated by 1 mM ATP for 5 min. on peritoneal macrophages from 30-37 ºC. Adding BBG (100 nM) or the selected 1,2,3-triazole derivatives when incubating for 10 min. of the total. The initial 5 min. during which the antagonists were added alone and the last 5 min. in conjunction with ATP. (B) The plot represents the quantification of the data observed in A; the % relative current recorded as a function of the ratio between the amplitude of the ionic current and the cell capacitance. The values represent the mean ± SEM of the total % ATP effect. The profiles are representative of 3-6 independent experiments for whole cell recordings.

Table 8. Antagonistic effect of triazoles in mice P2X7R.

P2X7R antagonists and Triazoles	*IC_{50} (µM)
BBG	**0.109**
05e	0.341
06a	0.103
08h	0.103
09d	0.069

09i	0.316
11	0.457
12	0.081

*IC_{50} values were obtained from whole cell configuration. Data values are expressed as means ± SDs. All experiments were repeated at least 3 times.

Cytotoxicity of the selected triazoles. Cytotoxicity in MPM was measured in crescent selected triazole analogue concentrations as shown in Fig. 5 after continuous exposition for 24 hours. Triazoles **5e**, **9i**, and **11** caused cell toxicity at 362 µM, 505 µM and 250.2 µM, respectively. By contrast, analogs **6a**, **8h**, **9d** and **12** reached their CC_{50} at 3.73 mM, 2.84 mM, 4.04 mM and 2.35 mM, respectively (Fig. 5 and Table 9). Triazoles **6a**, **8h**, **9d** and **12** exhibit cytotoxicity effect in concentrations at least 1,000 times lower than IC_{50} values. Therefore, they are good candidates to continue the studies.

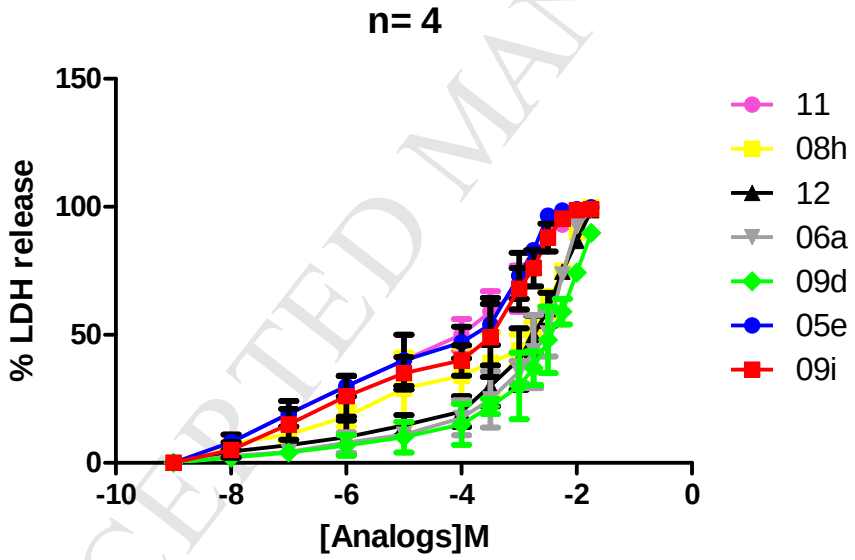

Fig. 5. Toxicity of selected 1,2,3-triazole derivatives on mouse peritoneal macrophages. The dose response curve of selected 1,2,3-triazole derivatives to peritoneal macrophages at concentrations ranging from 1 nM - 10 mM for 24 h. The profiles are representative of 3-6 independent experiments

Table 9. Cytotoxicity of selected triazoles in mice P2X7R.

P2X7R antagonists and Triazoles	*CC_{50} (µM)
05e	**0.363**
06a	3.739
08h	2.841

09d	4.032
09i	0.505
11	0.250
12	2.357

*CC_{50} values were obtained from LDH assay in MPM. Data values are expressed as means ± SDs. All experiments were repeated at least 3 times.

Antagonist action of the selected triazoles derivatives against HEK-293 cells transfected with P2X7R. As MPM express other P2XR, we used transfected cells to confirm the P2X7R inhibition. Then, we used dye uptake assay in fluorescent plate reader to evaluate the antagonist action of human P2X7R transfected to HEK-293 cells. All selected triazoles inhibited ATP-induced ethidium uptake (Table 10). However, when compared to mouse receptor in MPM, only the triazole **9d** displayed a potency higher than A740003 (86 nM) to inhibit transfected cells (Table 10) and with IC_{50} values similar in both models (83.40 nM in mouse and 5.3 nM in human). Additionally, tetrazole derivatives have generated compounds with high potency to inhibit P2X7R [57,77]. As only the analog **9d** demonstrated inhibition superior to A740003 antagonist to inhibit hP2X7R mediated dye uptake, we selected this molecule to continue the experiments.

Table 10. Antagonistic effect of triazole derivatives in HEK-293 cells transfected with human P2X7R

P2X7R antagonists and triazole derivatives	IC_{50} (µM)
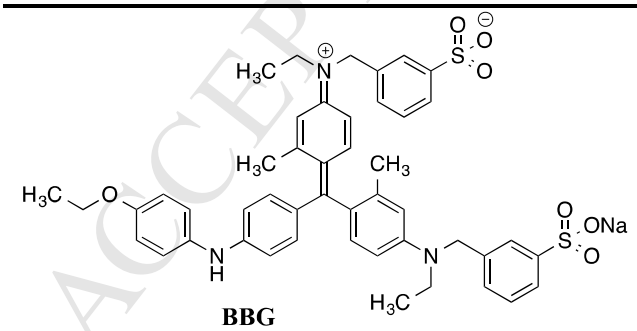 **BBG**	0.552
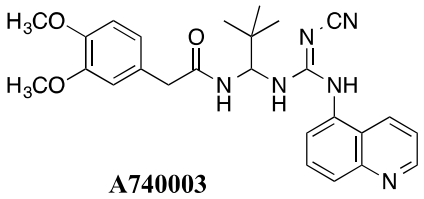 **A740003**	0.086
5e	0.932
6a	0.478
8h	0.108

9d	0.0053
9i	0.621
11	0.897
12	0.522

*IC_{50} values were obtained from concentration-response curves in ethidium uptake assay. Data values are expressed as means ± SDs. All experiments were repeated at least 3 times.

*The triazole derivative **9d** inhibits competitively the BzATP and ATP induced P2X7R function on MPMs.* BzATP when compared with ATP, had its effect inhibited by **9d** in dye uptake assay and macroscopic ionic currents measurements (Fig. 6). In comparison to BBG (IC_{50} 431.6 nM) and the selective P2X7R antagonist, A740003 (IC_{50} 63.33 nM), the triazole **9d** inhibited BzATP (100 µM) induced ethidium uptake in lower IC_{50} value, 59.18 nM (Fig. 6A). BzATP-induced P2X7R macroscopic currents also demonstrated the same inhibitory profile, BBG (IC_{50} 407.2 nM), A740003 (IC_{50} 46.91 nM) and **9d** (IC_{50} 41.09 nM) (Fig. 6B). We investigated the hypothetical mechanism of inhibition of the **9d** triazole through electrophysiological assay on MPMs. We applied ATP (Fig. 6C) or BzATP (Fig. 6D) in crescent concentration alone or in the presence of 500 nM **9d**. Both agonists, in the presence of the compound **9d,** augmented their concentrations about 10 times to reach an effect similar to agonists alone. These profiles indicate compound **9d** as a competitive antagonist (Fig.s 6C and 6D).

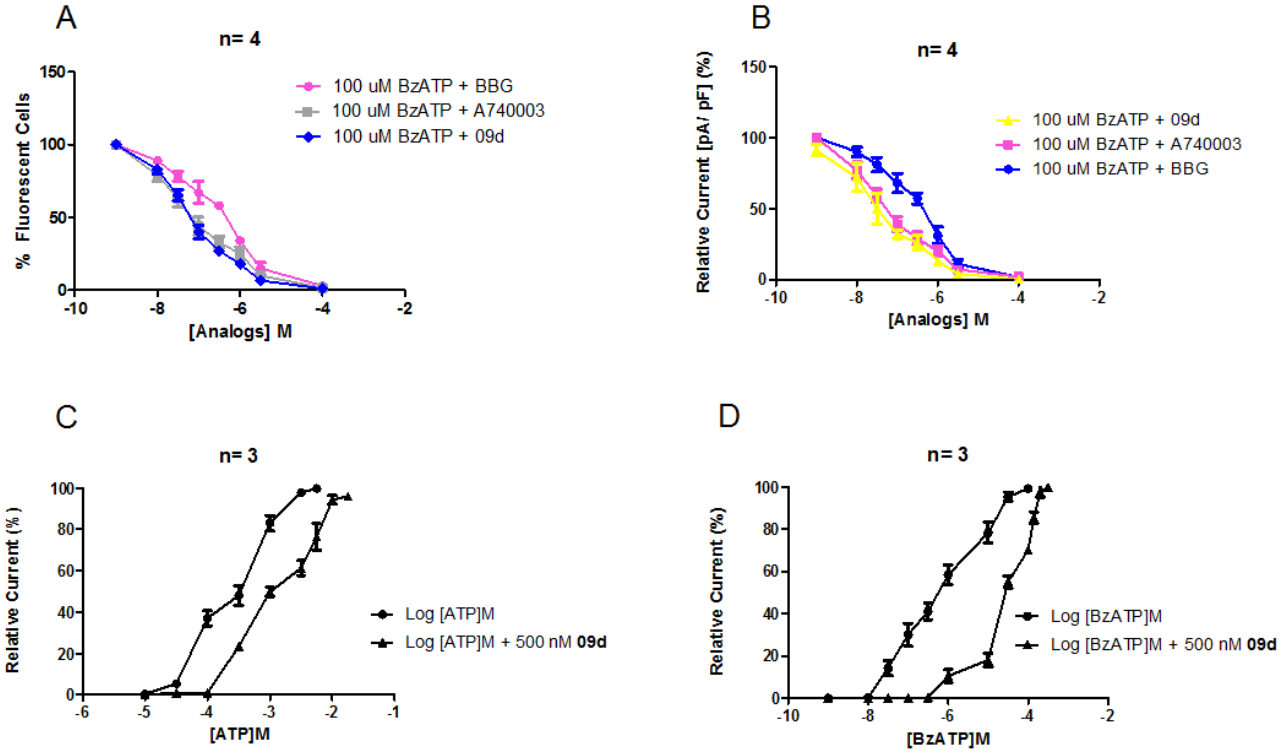

Fig. 6. Analog **9d** decreased BzATP induced dye uptake and ionic currents and competitively inhibit P2X7R in MPM. (A) Dose-response curve to dye uptake of BBG, A740003 and **9d** triazole in the presence of 100 µM BzATP. (B) Dose-response curve to ionic currents of BBG, A740003 and **9d** triazole in the presence of 100 µM BzATP. (C) Dose-response curve comparing ATP concentrations alone and in the presence of a fixed dose of 500 nM **9d**. (D) Dose-response curve comparing BzATP concentrations alone and in the presence of a fixed dose of 500 nM **9d**. The profiles are representative of 3 separate experiments in distinct days.

*The triazole derivative **9d** inhibits IL-1β release mediated by P2X7R activation in differentiated THP-1 cells.* Another outstanding P2X7R function is the IL-1β release. Differentiated THP-1 cells treated with LPS (100 ng/mL) during 4 hours and stimulated with ATP (1 mM) for 15 minutes exhibited dose-dependent reduction of the IL-1 β release with IC_{50} of 67.46 ± 3.77 nM, after treatment with **9d** triazole. The triazole **9d** showed IC_{50} value minor than A740003 to inhibit this hP2X7R as observed for other parameters tested above (Table 11).

Mice peritoneal macrophages stimulated with LPS (100 ng/mL) during 4 hours and treated with ATP (1 mM) for 15 minutes also was inhibited by **9d** treatment with IC_{50} value of 91 ± 4.6 nM (Table 11). The **9d** inhibition also was higher than A740003 in mP2X7R.

Table 11. Antagonistic effects of **9d** triazole against ATP-induced IL-1β release in LPS/IFNc-differentiated human THP-1 cells

P2X7R antagonist and triazole derivative	THP-1 cells IC_{50} (µM) IL-1β release	HEK-293 cells transfected with hP2X7R IC_{50} (µM) IL-1β release	Mice Peritoneal macrophages IC_{50} (µM) IL-1β release
A740003	0.089	0.082	0.112
9d	0.067	0.067	0.091

• *IC_{50} values were obtained from concentration-response curves. Data values are expressed as means ± SDs. All experiments were repeated at least 3 times

3.2.2. In Silico

ADMET properties

The anti-inflammatory property observed for triazole derivative **9d** in vivo (Figs. 7 and 8) increase the possibility to therapeutic application. Based on these results, we used Osiris software to predict the physicochemical values for compound 9d in comparing to commercial anti-inflammatories drugs (diclofenac, ibuprofen and naproxen) as well as the main toxicological parameters for 9d analog in which indicate low risk of mutagenic, tumorigenic, irritable properties or interference of reproduction process.

The compound **9d** has a molecular weight similar to naproxen and topological polar surface area similar to ibuprofen, however it has a lower lipophilicity and a higher solubility in water than the compared drugs (Table 12). The pharmacokinetic parameters (calculated using ADMET Predictor® - Simulation Plus) of the compound 9d comparing to the same commercial anti-inflammatories drugs have the same profile as blood brain barrier and human intestinal absorption, though a different affinity to plasma protein binding (Table 12).

Table 12. Physical-chemical and pharmacokinetics parameters of compound 9d in comparing to commercial anti-inflammatories drugs (diclofenac, ibuprofen and naproxen)

Compound	Physical-chemical Properties				Pharmacokinetics Parameters		
	MW[a]	LogP[b]	LogS[c]	TPSA[d]	BBB[e]	HIA[f]	NBPP[g]
9d	237	1.37	-2.41	39.94	high	high	8.32
diclofenac	295	3.89	-4.64	49.33	high	high	0.38
ibuprofen	206	3.0	-2.89	37.30	high	high	2.10
naproxen	230	2.69	-3.59	46.53	high	high	1.33

[a]Molecular weight (Da); [b]Partition coefficient in a logarithmic scale; [c]Solubility in water coefficient in a logarithmic scale; [d]Topological Polar Surface Area; [e]Blood brain barrier; [f]Human intestinal absorption; [g]Non-binding protein plasma

An important step in the development of bioactive compounds is to study what the human organism does with the compound, so we investigated the enzymes involved in metabolism. CYP isoforms are major enzymes in drug metabolism. Compound **9d** may be metabolized by CYP1A2, while diclofenac, ibuprofen and naproxen have more probability to be metabolized by CYP2C9 (Table 13). UDP-glucuronosyltransferase isoforms, responsible to catalyze conjugation reactions, may acts on the compound 9d by UGT1A4, while the compared drugs may be metabolized mainly by UGT1A3 and UGT2B7.

Table 13. Qualitative evaluation of the compound **9d** as well as commercial anti-inflammatories drugs (diclofenac, ibuprofen and naproxen) of being metabolized by the main CYP and UDP-glucuronosyltransferase isoforms

Compound	CYP isoforms					UGT isoforms								
	1A2	2C9	2C19	2D6	3A4	1A1	1A3	1A4	1A6	1A8	1A9	1A10	2B7	2B15
9d	yes	no	no	no	no	no	no	yes	no	no	no	no	no	no
diclofenac	no	yes	no	no	no	no	yes	no	no	no	no	no	yes	no
ibuprofen	no	yes	no	no	no	no	yes	no	yes	no	yes	no	yes	no
naproxen	no	yes	no	no	no	yes	yes	no	yes	no	yes	no	yes	no

3.2.3. Solubility, microsomal stability and permeability in vitro

*Solubility, Liver Microsomal Stability and Caco-2 cells permeability of **9d***. Triazole **9d** was tested for microsomal stability in mice and human liver microsomes, and assessed for permeability in a Caco-2 assay. This triazole seemed to be stable in mice and human microsome assays (Table 14). Compound **9d** exhibited an intermediary Intrinsic Clearance (CLint) for mouse and human microsomes [78]. Additionally, **9d** was permeable for Caco-2 in percentage above to 70% (Table 14) when compared as propanolol.

Table 14. Liver microsomal stability and Caco-2 data for **9d**.

Liver Microsomes	LM stability(a)	Caco-2(b)
Mouse	22.2	
Human	30.2	77.41 ± 1.77

(a) Stability in mice and human liver microsomes. Data reported as CLint (µL/min/ mg protein).

(b) Apparent permeability values (Papp) measured using as reference with low permeability vinblastine and high permeability propranolol absorption compounds. Data reported in 10^6 cm/s. These values are referent to apical to basolateral (A-B) direction. They were tested at the same time as **9d**. Values are means ± standard error of 3 experiments.

When solubilized in pH values ranging from 2 to 10, in all cases **9d** demonstrated solubility above to 250 µM (Table 15). $LogD_{7.4}$ gave a value of -1.96 ± 0.23 (Table 16). This reduced lipophilicity favored microsomal stability and almost did not affect Caco-2 permeability results measured (compare Table12 with Tables 13 and 14).

Table 15. Solubility of **9d** at various pH conditions.

Drug	pH 2(a)	pH 4(b)	pH 7.4(c)	pH 10(d)
9d	<250 µM	<250 µM	<250 µM	<250 µM

(a) pH 2: hydrochloride buffer; (b) pH 4: citrate buffer; (c) pH 7.4: phosphate buffer; (d) pH 10: sodium hydroxide buffer, n= 3 in distinct days.

Table 16. Log D of **9d** triazole.

Compound	$LogD_{7.4}$ (a)
9d	-1.96 ± 0.23

(a) Results are average of three experiments and in all cases individual Log D values were within ± 0.3 log unit of average Log D Propranolol HC.

3.2.4. In Vivo

Based on *in vitro* results, compound **9d** inhibitory activity was tested in a mouse paw edema model induced by ATP [79] or carrageenan [80]. In this assay to observe an inflammation model strictly stimulated by a purinergic mechanism, 1 mM ATP was applied to the paws and edema formation was measured after 30 minutes. As expected, ATP induced edema formation was inhibited by **9d** triazole with ID_{50} value of 79.84 ng/kg (Fig. 7A). Paw edema formation induced by carrageenan, a general pro-inflammatory agent, also was inhibited by **9d** triazole in a dose-dependent manner (Fig. 7B) with an ID_{50} value of 94.35 ng/kg. Oral administration of **9d** inhibited ATP and carrageenan- induced paw formation with higher potency than intraperitoneal treatment. ID_{50} values for oral treatment were 68.59 ng/kg^{-1} and 80.49 ng/kg-1, respectively (Fig. 7C and D). All treatments with **9d** promoted paw edema inhibition more potent than A740003 P2X7R antagonist (Fig. 7).

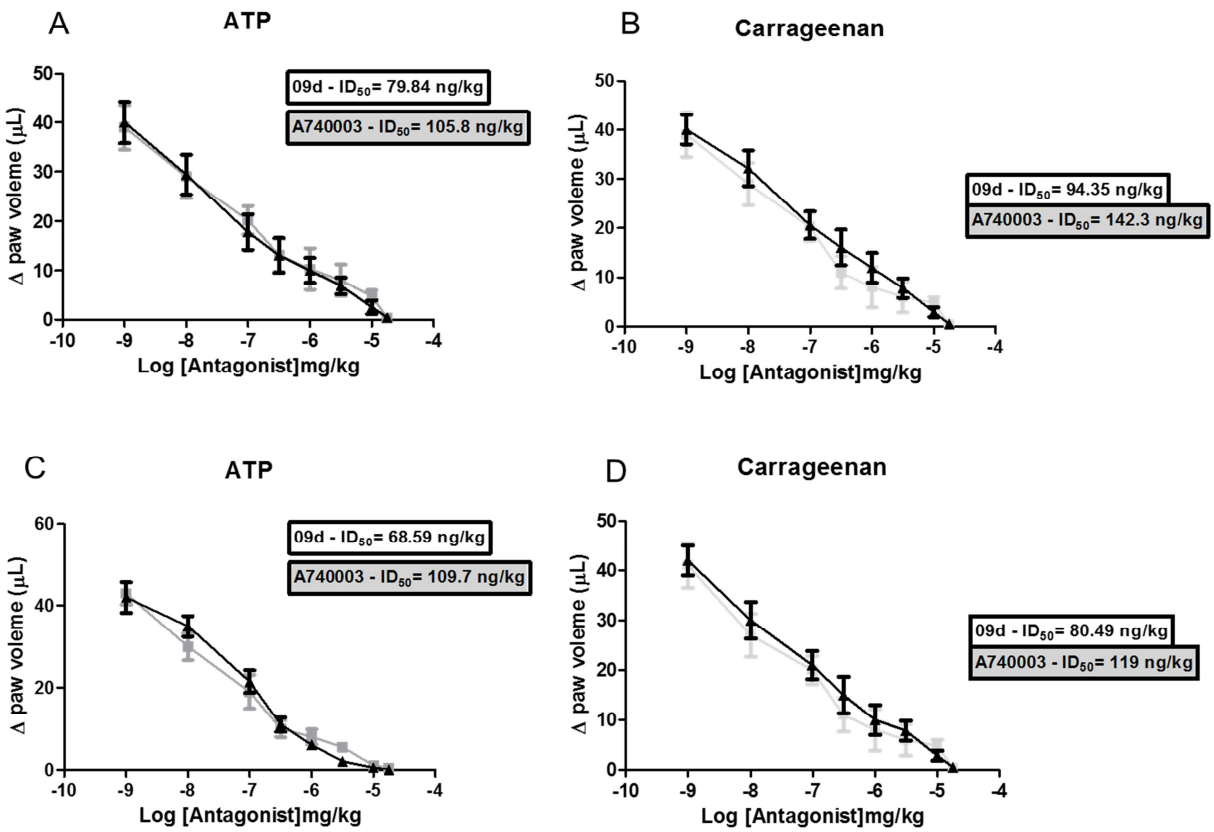

Figure 6

Fig. 7. *In vivo* inhibition of paw edema formation by the **9d** derivative in mice. (A) Dose-response curve between **9d** doses and paw edema formation after ATP (1 mM) treatment in the paw. The mice were pretreated for 1 h with **9d** derivative in crescent concentrations administrated by intraperitoneal pathway. Paw edema was measured 30 min after ATP application. (B) Dose-response curve between **9d** doses and paw edema formation after carrageenan (300 uM) treatment in the paw. The mice were pretreated for 1 h with **9d** derivative in crescent concentrations administrated by intraperitoneal pathway. (C) Dose-response curve between **9d** doses and paw edema formation after ATP (1 mM) treatment in the paw. The mice were pretreated for 1 h with **9d** derivative in crescent concentrations administrated by oral pathway. Paw edema was measured 30 min after ATP application. (D) Dose-response curve between **9d** doses and paw edema formation after carrageenan (300 uM) treatment in the paw. The mice were pretreated for 1 h with **9d** derivative in crescent concentrations administrated by oral pathway Paw edema was measured 60 min. afterwards. These results are representative of 3-5 experiments that were performed on distinct days

We have also evaluated the anti-inflammatory activity of **9d** in the model of LPS-induced pleurisy. The treatment with diclofenac or **9d** inhibited LPS-induced the pleural accumulation of total leucocytes (Fig. 8A) and mononuclear cells (Fig. 8B), in contrast to neutrophils (Fig. 8C) and eosinophils (Fig. 8D). The protein extravasation induced by LPS stimulation was inhibited by 100 ng/kg **9d**, whereas diclofenac did not alter the response (Fig. 8E). Nitric oxide production was not inhibited by diclofenac, however **9d** analog reduced nitrite levels in treated mouse pleural washes (Fig. 8F).

Thus, triazole derivative **9d** potently reduced acute topical inflammation induced by ATP or carrageenan and in minor proportion the acute airways inflammation induced by LPS. These results are promisor because **9d** effects occur in nanomolar concentrations, as observed for other potent commercial P2X7R antagonist [26,27,81].

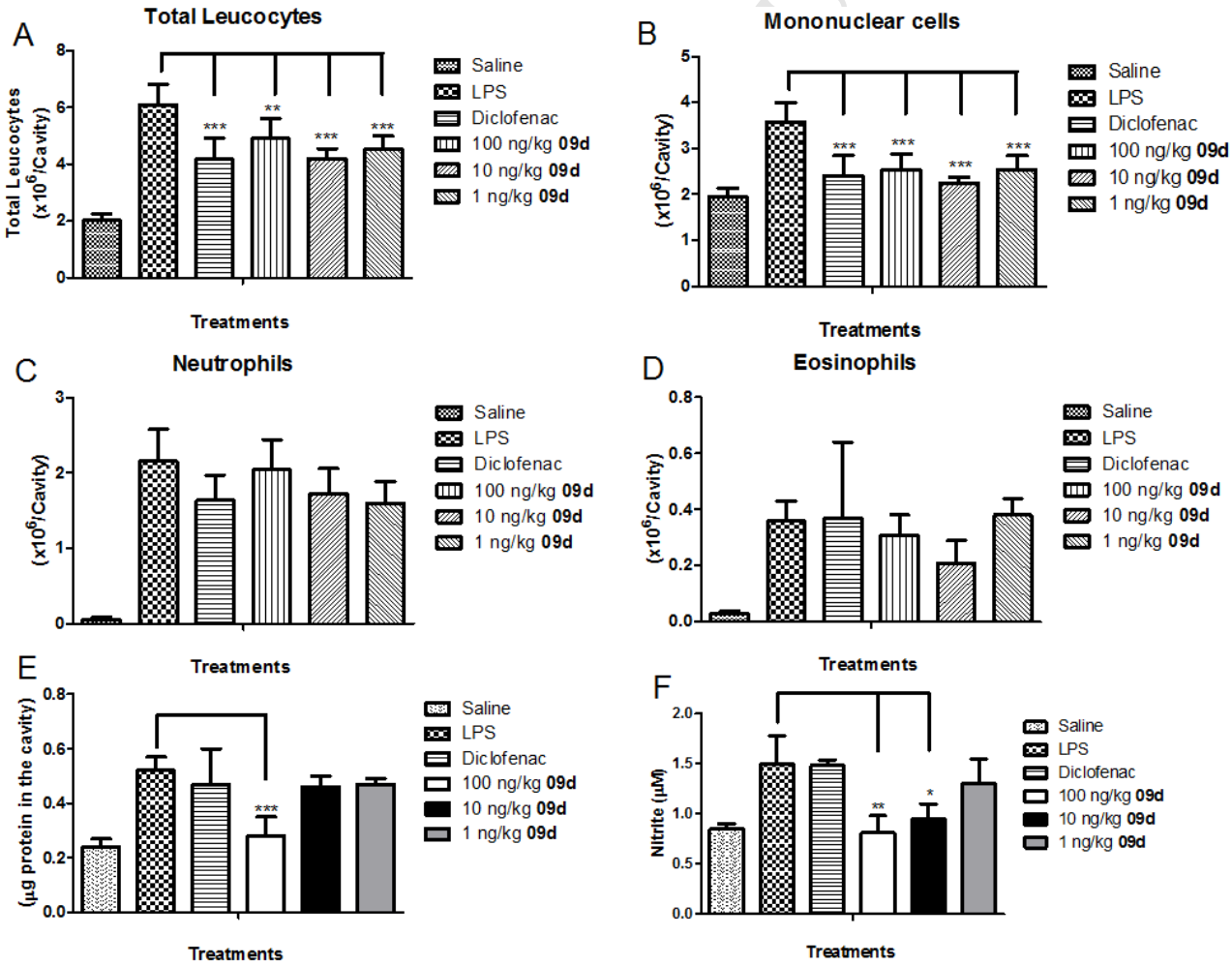

Fig. 8. Inhibition of LPS-induced pleurisy in mice by analog **9d**. Mice were pre-treated with diclofenac (100 mg/kg, i.p.) or with **9d** derivative (1-100 ng/kg, i.p.) for 1 h before LPS stimulation (250 ng/cav., i.t.). After 24 h after stimulation, the number of (A) total leucocytes, (B) mononuclear cells, (C) neutrophils, (D) eosinophils were evaluated in pleural washes. (E) Total protein and (F) nitrite were determined in pleural washes by Lowry and Griess methods, respectively. Results are representative of three independent experiments with five animals per group

3.2.5. Molecular Docking

According to our experimental investigation, the results indicated P2X7R inhibition in the presence of compound **9d**. Additionally, ATP concentration to reach the maximal response was higher in comparison to ATP alone. These observations suggest compound **9d** acting by a competitive inhibition mechanism.

Based on these results, we performed a molecular docking of the three most potential inhibitors (**9d**, **8h** and **12**) in the ATP binding pocket as the potential target to study its possible binding mode and explore the most relevant interactions among them. Molecular docking approach suggested a very similar binding mode for all three inhibitors. Fig. 9 depicts the superposition of the best binding pose of the analogs **9d**, **8h** and **12** in the structure P2X7 ATP binding site. It is possible to note that the probable binding mode of the compounds is interacting theirs 1,2,3-triazole moiety with the highly conserved residues in the ATP binding site in addition with theirs chlorobenzene/benzene ring orientated toward the narrow apolar end of the ATP binding site.

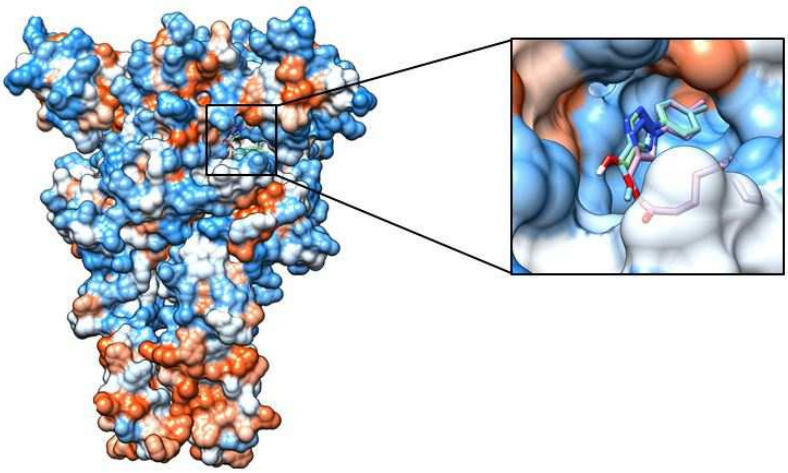

Fig. 9. Superposition of the three most potent inhibitors (**9d**, **8h** and **12**) into the human P2X7R. In blue are depicted polar regions and in orange are depicted the apolar regions. Illustration generated by UCSF *Chimera* program [82].

Inhibitor orientation in the ATP binding site is mainly governed by the hydrogen bond between conserved residues such as Lys311 and Ans292 from subunit α with the oxygen and/or triazole nitrogen of the compounds. Considering that those residues are highly conserved and known to interact with the ATP substrate, this molecular docking supports a potential competitive characteristic of these inhibitors (Fig. 10). In addition, is possible to note that whereas 9d and 8h makes two hydrogen bonds, **12** makes only one hydrogen bond. Such aspect can be related to the difference in binding affinities. Indeed, compounds **9d** and **8h** showed the lowest IC_{50} values in the experimental test with HEK293 cells transfected with human P2X7R.

Another relevant feature of the binding site that guides the referred ligands orientation is the narrow and apolar end of the ATP binding pocket, which makes hydrophobic interactions with the aromatic ring of the ligands, mainly by the lateral chain of the Val173 and Lys145, thus increasing the binding affinity. Furthermore, the introduction of the chlorine atom in the aromatic ring (such as compounds **9d** and **8h**) can also contribute for gains in binding free energy, by increasing the amount of hydrophobic surface buried into the binding pocket. Further, the aliphatic chain of the compound **8h** makes weak hydrophobic interaction with Pro289 and Pro142 from subunit α, thus indicating more mobility and less interaction, therefore contributing to favorable entropy binding.

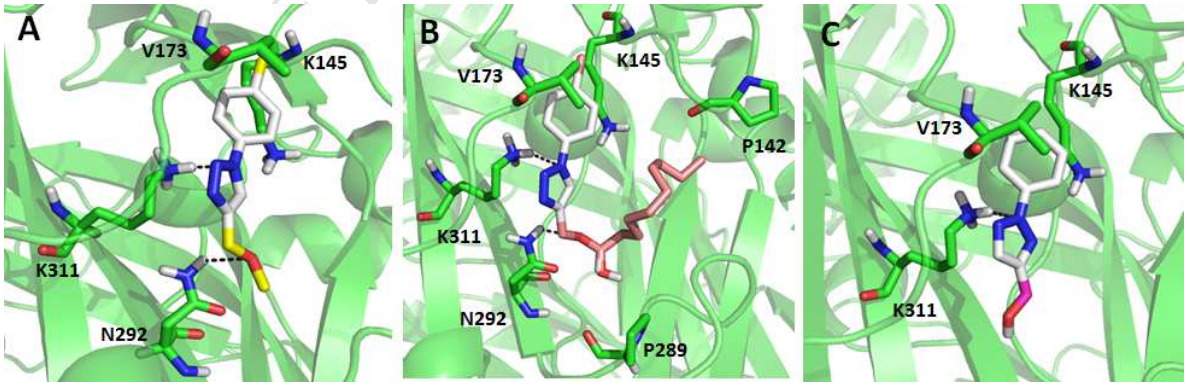

Fig. 10. Depiction of the inhibitors binding pose, obtained by molecular docking, into P2X7R ATP binding site: (A) compound **9d**, (B) compound **8h** and (C) compound **12**. In green is represented the receptor P2X7 and highlighted in stick are depicted the main residues involved in the interaction with the inhibitors. Illustration generated by PyMOL program.

4. Discussion

Although there are a large number of P2X7R antagonists commercially available, research of novel molecules with antagonist and therapeutic action on this receptor is necessary. First-generation P2X7R antagonists (Suramin, PPADS, BBG, KN-62 and Reactive blue-2) are non-selective inhibitors, acting also on other P2Rs [26] or in proteins related to P2X7R pore formation mechanism [6]. The second generation of P2X7R antagonists includes JNJ-47965567 [27], A740003 [28], GSK314181 [29], triazole derivatives A438079 [30], A839977 [31], AZ11645373 [81], AZ10606120 [32] and AZD9056 [33]. Characterization of their mechanisms of action and pharmacologic properties *in vivo* indicate possibly for inhibiting allosterically [70]. In some cases, they exhibit reduced availability and variable potency according to the species studied [26].

Clinical trials using P2X7R antagonists against rheumatoid arthritis indicated clinical efficacy and safety of the P2X7R antagonists AZD9056 or CE-224,535 [33,34]. In contrast, both trials did not exhibit therapeutic benefit [33,34]. A possible explanation is associated to studies related to differential pharmacological sensibility in P2X7R genotype function, as observed by McHugh and collaborators *in vitro* [35]. This scenario leaves open a possibility to search and develop novel P2X7R antagonists.

We evaluated the effects of 1,2,3-triazole derivatives on P2X7R present in peritoneal macrophages and HEK-293 transfected with human P2X7R *in vitro* and ATP-induced the paw edema and pleurisy *in vivo*.

All triazoles initially were tested in the concentration of 10 µM and its cytotoxic effects in this dose were evaluated by lactate dehydrogenase (LDH) release assay. Initial screening of 1,2,3-triazole derivatives was done using dye uptake assay on peritoneal macrophages using FLIP to detect the fluorescence. We selected seven derivatives (**5e**, **6e**, **8h**, **9d**, **9i**, **11**, **12**), which presented IC_{50} values inferior to BBG to inhibit dye uptake or ionic currents (Fig. 3-4). Dose-response curves obtained for electrophysiology and dye uptake measured by flow cytometry assay displayed nanomolar potency for all triazoles selected. Among them, **9d** exhibited, in both assays, the minor concentration able to inhibit 50% of effect (IC_{50}) values of 69 nM and 83 nM, respectively. HEK-293 cells transfected with human P2X7R confirmed the action of the compounds against P2X7R with IC_{50} value of 5,3 nM for dye uptake assay. Triazole derivatives IC_{50} values are comparable to values observed for P2X7R antagonists available in the commercial to inhibit the mice P2X7R and human P2X7R [26,81,83-85]. In relation to **9d** derivative, its inhibition was more potent than BBG, KN-62, A438079, A740003, AZ10606120 and AZ11645373 in the mice P2X7R *in vitro* [26,27,83]. In this context, triazole/tetrazole derivatives were initially indicated as P2X7R antagonists from a

high-throughput screen (HTS) in the recombinant human cell line. Structure-activity relationship (SAR) studies of tetrazole analogues in a rat model of neuropathic pain identified the 1-benzyl-5-(2,3-dichlorophenyl)-tetrazoles as potent antagonists [86]. The pIC_{50} value measured was of 6.9.

In 2007, Carrol and colleagues promoted substitutions in a tetrazole core inserting triazole isostere. Triazole-based P2X7 antagonists showed potency (pIC_{50} 6.43-7.12) and physiochemical properties improved in comparison to tetrazole analogues [59]. Based on assays above, Florjancic and collaborates used SARs to search the aminotriazole activity at both human and rat P2X7R. In consequence, they observed drugs with pIC_{50} value in turn of 7.5 to block both receptors [60].

Honore [31] demonstrated *in vitro* and *in vivo* the inhibitory activity of a structurally novel P2X7R antagonist, 1-(2, 3-dichlorophenyl)-*N*-[2-(pyridin-2-yloxy) benzyl]-1*H*-tetrazol-5-amine (A-839977) in mice. A-839977 inhibited BzATP-evoked calcium influx at recombinant human, rat and mouse P2X7Rs. The IC_{50} values varied from 20-150 nM for Ca^{2+} assay, $pIC_{50} = 8.18 \pm 0.03$ for dye uptake and $pIC_{50} = 7.43 \pm 0.13$ to IL-1β release assay.

The *in vitro* toxicity measured by LDH release assay ruled out analogs **5e**, **9i** and **11**, because they exhibited toxicity in micromolar concentrations (Fig. 5). In the other hand, the CC_{50} values observed for **6a**, **8h**, **9d** and **12** were in a 1000 times superior to IC_{50} values measured in different assays (Fig. 5).

HEK-293 cells transfected with hP2X7R demonstrated that analogs **12** and **6a** displayed IC_{50} values comparable to BBG, however they were at least 5 times less potent than A740003. The derivative **8h** exhibited an IC_{50} value higher than A740003. Additionally, only the analog **9d** displayed IC_{50} value reduced in comparison to A740003 to inhibit hP2X7R dye uptake (Table 4). This triazole was the unique able to inhibit hP2X7R in concentrations inferior to 10 nM and potent inhibition in both species.

Carrol and collaborates in 2007 showed a potency reduction to inhibit intracellular Ca^{2+} influx mediated by P2X7R in the following order: tetrazole>triazole>pyrazole>imidazole in according to heterocyclic core in this pharmacophore [57]. Posterior publication producing aryl substitutions in the compounds above produced aryltetrazoles A-438079, the compound **6** with hP2X7 $pIC_{50} = 6.3$ and aryltriazoles as the compound 44 with (hP2X7 pIC_{50} 7.1). These substituents did not cause relevant augment in the potency observed [58]. In a general manner, **9d** compound exhibited inhibitory activity in values inferior to registered in these papers. Rudolph and collaborates described series of methyl substituted 1-(5,6-dihydro-[1,2,4]triazolo[4,3-a]pyrazin-7(8*H*)-yl)methanones with elevate potency in rat and human P2X7R.

Some compounds inhibited also in concentrations low to 10 nM, the P2X7R of both species and they reached high P2X7R occupancy in rat following oral administration [87]. Savall and

colleagues studied 1,2,3-triazolopiperidines with brain penetrant properties. They produced compounds with high potency to hP2X7R and rP2X7R, similar to observed with **9d** triazole. These triazolopiperidines were no toxic and had good physicochemical parameters with bound in the rP2X7R *in vivo* [88]. Differential potency to inhibit P2X7R among species is related to diverse classical and second generation antagonists [80,88-90] and fused 1,2,3-triazole analogs [91]. Therefore, analog **9d** shows a promising antagonistic activity against P2X7R.

In MPM, there are other P2X receptors associated to pore formation and able to uptake fluorescent dyes, then we used BzATP, which is a more potent P2X7R agonist compared to ATP [92]. BzATP induced dye uptake and ionic currents were inhibited by BBG and A740003, both P2X7R antagonists. The molecule **9d** inhibited BzATP effect with IC_{50} value inferior to these P2X7R antagonists (Figs. 5A and 5B). This agonist, BzATP, also could activate other P2XRs [93], but its effect 10 times more potent than ATP associated to A740003 antagonism, because it is selective to P2X7R [28], support the P2X7R as main receptor responsible to effects observed in our model.

Based on these results, we did a competitive assay comparing ATP or BzATP concentrations alone and this condition in the presence of a unique dose of **9d** analog related to ionic currents mediated by P2X7R activation (Fig. 6C and 6D). The right shift of the curve with antagonist augmenting in 10 times the concentration necessary to promote the same effect showed in the absence of the **9d** triazole observed in both graphs sustain a competitive action of this molecule. Besides that, molecular docking indicated a similar binding mode for the three most potent compounds in the ATP pocket, in which theirs 1,2,3-triazole moiety interact by hydrogen bond with the highly conserved residues in the ATP binding site, such as K311 and N292. Hence, indicating the relevance of this triazole moiety for the compounds bioactive conformation.

IL-1β release also was inhibited by **9d** with IC_{50} of 67 nM. In function of P2X7R participation promoting pro-inflammatory responses, we used to distinct inflammatory models to evaluated the potential of this triazole to act as anti-inflammatory drug. Compound **9d** inhibited ATP and carrageenan induced paw edema formation, the dose to inhibit 50% of effect (ID_{50}) values measured were 79.84 ng/kg and 142.3 ng/kg, respectively. These results show **9d** as a potent P2X7R antagonist *in vitro* and in general inflammatory reaction *in vivo*.

These data confirmed in vitro assays analyzing **9d** solubility, stability in liver microsomal metabolic stability indicating a moderate solubility and high quantity permeable and free to binding to P2X7R (Tables 12-14). Good characteristics to oral drug with therapeutic action.

Based on this data, a large number of papers describe pro-inflammatory characteristic of the P2X7R *in vitro* and *in vivo* and the search for new therapeutic drugs supported for its inhibition.

Thus, we did in vivo experiments in paw edema model. For this, we administrated ATP to realize a model in vivo with essential purinergic component [79]. This compound was evaluated *in vivo* for a model of ATP-evoked mice paw edema with two different agents, ATP (inflammation based on purinergic signaling) and the general pro-inflammatory carrageenan (COX dependent signaling). This derivative potently inhibited both inflammatory reactions with ID_{50} of 79.84 ng/kg^{-1} to ATP-induced paw edema and 94.35 ng/kg^{-1} to carrageenan-induced paw edema. These inhibition values were extremely lower compared to A740003 (IC_{50} = 105.8 and 142.3 ng/kg^{-1}, respectively) observed in the ATP and carrageenan-induced paw edema (Fig. 7) [81]. In according to pharmacokinetic characteristics, we also did oral administration using the same doses of intraperitoneal treatment. Oral treatment with **9d** reduced ATP-induced paw edema with ID_{50} of 68.59 ng/kg^{-1} and carrageenan-induced paw edema with ID_{50} value of 80.48 ng/kg^{-1} (Fig. 6C and D). This concentration range after oral or intraperitoneal treatment was similar to observed for other second generation of P2X7R antagonists [94,95].

Rats and mice thermal hyperalgesia induced by intraplantar administration of complete Freund's adjuvant (CFA) were impaired by systemic administration of A-839977. They measured an ED_{50} value of 100 μmol/kg intraperitoneal in rats and 40 μmol/kg, intraperitoneal in mice [32]. Pleurisy, another animal model, was used to evaluate the anti-inflammatory effect of **9d** analog, by using LPS, a potent pro-inflammatory stimulus that triggers the production of a wide range of chemoattractant mediators and leads to leukocyte accumulation in inflamed pleura.

The pre-treatment with analog **9d (**1-100 ng/kg) reduced LPS-induced total leucocytes and mononuclear cell influx into mouse pleural cavity, protein extravasation and NO production (Fig. 8). Our results are similar to previous reports that show the reduction of LPS-induced inflammation in mice treated with the P2X7 receptor antagonists BBG, oxidate ATP [76] and A438079 [96]. Additionally, these results support new experiments to study toxicological and therapeutical properties of the **9d** triazole. *In silico* evaluation indicated a low toxicological potential as well as a favorable pharmacokinetics profile of **9d** compared with commercial anti-inflammatories drugs (diclofenac, ibuprofen and naproxen), in which **9d** indicates a less extend plasma protein binding and despite the fact that **9d** presented a lower LogP comparing to the commercial drugs it showed a good absorption in addition with a high capability of crossing the blood brain barrier (Table 6). Although the compound **9d** presented different metabolic profile from the commercial anti-inflammatories drugs, all of them are predicted to be metabolized by at least one isoform of CYP oxygenases and by at least one isoform of UDP-glucuronosyltransferase, suggesting that the glucuronidation reaction is one route of elimination and inactivation of this compound (Table 7).

5. Conclusions

Supplementary studies will be necessary to verify the selective action to P2X7R, the potency among species, the *in vivo* toxicity and other pharmacological characteristics of the **9d** derivative. In conclusion, this bioactive compound shows a potent inhibition of the P2X7R cationic function and pore formation *in vitro. In vivo*, this substance also potently impaired the inflammatory reaction promoted by ATP, carrageenan or LPS in mice. Moreover, the molecular docking studies suggest a potential binding mode conformation for the three most potent inhibitors and contribute for new insights into structure active relationship of the compounds. The triazole derivative **9d** is a promisor P2X7R antagonist in mice with potential therapeutic.

Supporting information

Supporting information 1 includes physical and spectroscopic information for compounds **6c**, **7b**, **8l-q**, **9b**, **9e**, **9g**, **9h**, **9j**, **9k**, **9m**, **9n** and **14b**.

Acknowledgments

The authors are indebted to CNPq (National Council of Research of Brazil), CAPES and FAPERJ for funding this work and for Research fellowships.

Author Contributions

Performed the experiments (chemical synthesis): Daniel Tadeu Gomes Gonzaga.
Performed the experiments (biological assays): Leonardo Braga Gomes Ferreira, Thadeu Estevam Moreira Maramaldo Costa, Luiza Pereira Dantas, Hércules R. Freitas, Ricardo A. de Melo Reis, Ana Paula Sposito Simões, Juliana Carvalho Arruda and Paulo Anastácio Furtado Pacheco.
Wrote the paper: Carmen Penido, Vitor Francisco Ferreira, Robson Xavier Faria and Fernando de Carvalho da Silva.
In silico studies: Natalia Lidmar von Ranke, Murilo Lamim Bello, Helena Carla Casto, Carlos Rangel Rodrigues

Conflict of Interest

The authors declare that there are no conflicts of interest.

References

[1] G. Burnstock, Pathophysiology and therapeutic potential of purinergic signaling, Pharmacol. Rev. 58 (2006) 58-78.

[2] F. Jacob, C.P. Novo, C. Bachert, K. van Crombruggen, Purinergic signaling in inflammatory cells: P2 receptor expression, functional effects, and modulation of inflammatory responses, Purinergic Signal. (2013) 285-306.

[3] J.W. Booth, F.W. Tam, R.J. Unwin, P2 purinoceptors: Renal pathophysiology and therapeutic potential, Clin. Nephrol. 78 (2012) 154-163.

[4] G. Burnstock, F. Di Virgilio, Purinergic signalling and cancer, Purinergic Signal. 9 (2013) 491-540.

[5] A. Tuttolomondo, R. Di Sciacca, D. Di Raimondo, C. Renda, A. Pinto, G. Licata, Inflammation as a therapeutic target in acute ischemic stroke treatment, Curr. Top. Med. Chem. 9 (2009) 1240-1260.

[6] D.C. Broom, D.J. Matson, E. Bradshaw, M.E. Buck, R. Meade, S. Coombs, M. Matchett, K.K. Ford, W. Yu, J. Yuan, S.H. Sun, R. Ochoa, J.E. Krause, D.J. Wustrow, D.N. Cortright, Characterization of N-(adamantan-1-ylmethyl)-5-[(3R-amino-pyrrolidin-1-yl)methyl]-2-chloro-benzamide, a P2X7 antagonist in animal models of pain and inflammation, J. Pharmacol. Exp. Ther. 327 (2008) 620-633.

[7] N. Arulkumaran, R.J. Unwin, F.W. Tam, A potential therapeutic role for P2X7 receptor (P2X7R) antagonists in the treatment of inflammatory diseases, Expert Opin. Investig. Drugs 20 (2011) 897-915.

[8] T. Müller, R.P. Vieira, M. Grimm, T. Dürk, S. Cicko, R. Zeiser, T. Jakob, S.F. Martin, B. Blumenthal, S. Sorichter, D. Ferrari, F. Di Virgillio, M. Idzko, A potential role for P2X7R in allergic airway inflammation in mice and humans, Am. J. Respir. Cell Mol. Biol. 44 (2011) 456-464.

[9] M. El Ouaaliti, M. Seil, J.P. Dehaye, Activation of calcium-insensitive phospholipase A(2) (iPLA(2)) by P2X(7) receptors in murine peritoneal macrophages, Prostaglandins Other Lipid Mediat. 99 (2012) 116-123.

[10] I. Lemaire, S. Falzoni, B. Zhang, P. Pellegatti, F. Di Virgilio, The P2X7 receptor and Pannexin-1 are both required for the promotion of multinucleated macrophages by the inflammatory cytokine GM-CSF, J. Immunol. 187 (2011) 3878-3887.

[11] S. Muzzachi, A. Blasi, E. Ciani, M. Favia, R.A. Cardone, D. Marzulli, S.J. Reshkin, G. Merizzi, V. Casavola, A. Soleti, L. Guerra, MED1101: a new dialdehydic compound regulating P2X7 receptor cell surface expression in U937 cells, Biol. Cell 105 (2013) 399-413.

[12] R. Coutinho-Silva, P.M. Persechini, P2Z purinoceptor-associated pores induced by extracellular ATP in macrophages and J774 cells, Am. J. Physiol. 273 (1997) C1793-C1800.

[13] C.E. Gargett, J.E. Cornish, J.S. Wiley, ATP, a partial agonist for the P2Z receptor of human lymphocytes, Br. J. Pharmacol. 122 (1997) 911-917.

[14] M.P. Gehring, T.C. Brandão Pereira, R.F. Zanin, M.C. Borges, A.B. Filho, A.M.O. Battastini, M.R. Bogo, G. Lenz, M.M. Campos, F.B. Morrone, P2X7 receptor activation leads to increased cell death in a radiosensitive human glioma cell line, Purinergic Signal. 8 (2012) 729-739.

[15] T. Sugiyama, H. Kawamura, S. Yamanishi, M. Kobayashi, K. Katsumura, D.G. Puro, Regulation of P2X7-induced pore formation and cell death in pericyte-containing retinal microvessels, Am. J. Physiol. Cell Physiol. 288 (2005) C568-C576.

[16] R. Auger, I. Motta, K. Benihoud, D.M. Ojcius, J.M. Kanellopoulos, A role for mitogen-activated protein kinase (Erk1/2) activation and non-selective pore formationin P2X7 receptor-mediated thymocyte death, J. Biol. Chem. 280 (2005) 28142-28151.

[17] G.R. Dubyak, P2X7 receptor regulation of non-classical secretion from immune effector cells, Cell Microbiol. 14 (2012) 1697-1706.

[18] M. Barberà-Cremades, A. Baroja-Mazo, A.I. Gomez, F. Machado, F. Di Virgilio, P. Pelegrín, P2X7 receptor-stimulation causes fever via PGE2 and IL-1β release, FASEB J. 26 (2012) 2951-2962.

[19] C. Cervetto, S. Alloisio, D. Frattaroli, M.C. Mazzotta, M. Milanese, P. Gavazzo, M. Passalacqua, M. Nobile, G. Maura, M. Marcoli, The P2X7 receptor as a route for non-exocytotic glutamate release: dependence on the carboxyl tail, J. Neurochem. 124 (2013) 821-831.

[20] J.M. Teixeira, E.V. Dias, C.A. Parada, C.H. Tambeli, Intra-articular blockade of P2X7 receptor reduces the articular hyperalgesia and inflammation in the knee joint synovitis especially in female rats, J Pain. 18 (2017) 132-143.

[21] S. Apolloni, S. Amadio, C. Parisi, A. Matteucci, R.L. Potenza, M. Armida, P. Popoli, N. D'Ambrosi, C. Volonté, Spinal cord pathology is ameliorated by P2X7 antagonism in a SOD1-mutant mouse model of amyotrophic lateral sclerosis, Dis Model Mech. 7 (2014) 1101-1109.

[22] M. Monif, C.A. Reid, K.L. Powell, K.J. Drummond, T.J. O'Brien, D.A. Williams, Interleukin-1β has trophic effects in microglia and its release is mediated by P2X7R pore, J. Neuroinflammation 13 (2016) 173.

[23] T. Engel, R. Gomez-Villafuertes, K. Tanaka, G. Mesuret, A. Sanz-Rodriguez, P. Garcia-Huerta, M.T. Miras-Portugal, D.C. Henshall, M. Diaz-Hernandez, Seizure suppression and neuroprotection by targeting the purinergic P2X7 receptor during status epilepticus in mice, FASEB J. 26 (2012) 1616-1628.

[24] I.P. Chessell, J.P. Hatcher, C. Bountra, A.D. Michel, J.P. Hughes, P. Green, J. Egerton, M. Murfin, J. Richardson, W.L. Peck, C.B. Grahames, M.A. Casula, Y. Yiangou, R. Birch, P. Anand, G.N. Buell, Disruption of the P2X7 purinoceptor gene abolishes chronic inflammatory and neuropathic pain, Pain 114 (2005) 386-396.

[25] G. Lopez-Castejon, J. Theaker, P. Pelegrin, A.D. Clifton, M. Braddock, A. Surprenant, P2X(7) receptor-mediated release of cathepsins from macrophages is a cytokine-independent mechanism potentially involved in joint diseases, J. Immunol. 185 (2010) 2611-2619.

[26] A.D. Michel, S.-W. Ng, S. Roman, W.C. Clay, D.K. Dean, D.S. Walter, Mechanism of action of species-selective P2X(7) receptor antagonists, Br. J. Pharmacol. 156 (2009) 1312-1325.

[27] A. Bhattacharya, Q. Wang, H. Ao, J.R. Shoblock, B. Lord, L. Aluisio, I. Fraser, D. Nepomuceno, R.A. Neff, N. Welty, T.W. Lovenberg, P. Bonaventure, A.D. Wickenden, M.A. Letavic, Pharmacological characterization of a novel centrally permeable P2X7 receptor antagonist: JNJ-47965567, Br. J. Pharmacol. 170 (2013) 624-640.

[28] P. Honore, D. Donnelly-Roberts, M.T. Namovic, G. Hsieh, C.Z. Zhu, J.P. Mikusa, G. Hernandez, C. Zhong, D.M. Gauvin, P. Chandran, R. Harris, A.P. Medrano, W. Carroll, K. Marsh, J.P. Sullivan, C.R. Faltynek, M.F. Jarvis, A-740003 [N-(1-[(cyanoimino) (5-quinolinylamino) methyl]amino-2,2-dimethylpropyl)-2-(3,4-dimethoxyphenyl) acetamide], a novel and selective P2X7 receptor antagonist, dose-dependently reduces neuropathic pain in the rat, J. Pharmacol. Exp. Ther. 319 (2006) 1376-1385.

[29] M.A. Letavic, B. Lord, F. Bischoff, N.A. Hawryluk, S. Pieters, J.C. Rech, Z. Sales, A.I. Velter, H. Ao, P. Bonaventure, V. Contreras, X. Jiang, K.L. Morton, B. Scott, Q. Wang, A.D. Wickenden, N.I. Carruthers, A. Bhattacharya, Synthesis and pharmacological characterization of two novel, brain penetrating P2X7 antagonists, ACS Med. Chem. Lett. 4 (2013) 419-422.

[30] D.W. Nelson, R.J. Gregg , M.E. Kort, A. Perez-Medrano, E.A. Voight, Y. Wang, G. Grayson, M.T. Namovic, D.L. Donnelly-Roberts, W. Niforatos, P. Honore, M.F. Jarvis, C.R. Faltynek, W.A. Carroll Structure-activity relationship studies on a series of novel, substituted 1-benzyl-5-phenyltetrazole P2X7 antagonists, J. Med. Chem. 49 (2006) 3659-3666.

[31] P. Honore, D. Donnelly-Roberts, M. Namovic, C. Zhong, C. Wade, P. Chandran, C. Zhu, W. Carroll, A. Perez-Medrano, Y. Iwakura, M.F. Jarvis, The antihyperalgesic activity of a selective

P2X7 receptor antagonist, A-839977, is lost in IL-1alphabeta knockout mice, Behav. Brain Res. 204 (2009) 77-81.

[32] D.L. Donnelly-Roberts, M.F. Jarvis, Discovery of P2X7 receptor-selective antagonists offers new insights into P2X7 receptor function and indicates a role in chronic pain states, Br. J. Pharmacol. 151 (2007) 571-579.

[33] E.C. Keystone, M.M. Wang, M. Layton, S. Hollis, I.B. McInnes, Clinical evaluation of the efficacy of the P2X7 purinergic receptor antagonist AZD9056 on the signs and symptoms of rheumatoid arthritis in patients with active disease despite treatment with methotrexate or sulphasalazine, Ann. Rheum. Dis. 71 (2012) 1630-1635.

[34] T.C. Stock, B.J. Bloom, N. Wei, S. Ishaq, W. Park, X. Wang, P. Gupta, C.A. Mebus, Efficacy and safety of CE-224,535, an antagonist of P2X7 receptor, in treatment of patients with rheumatoid arthritis inadequately controlled by methotrexate, J. Rheumatol. 39 (2012) 720-727.

[35] S.M. McHugh, S. Roman, B. Davis, A. Koch, A.M. Pickett, J.C. Richardson, S.R. Miller, S. Wetten, C.J. Cox, F. Karpe, J.A. Todd, E.T. Bullmore, Effects of genetic variation in the P2RX7 gene on pharmacodynamics of a P2X(7) receptor antagonist: a prospective genotyping approach, Br. J. Clin. Pharmacol. 74 (2012) 376-380.

[36] R. Faria, L. Ferreira, R. Bezerra, V. Frutuoso, L. Alves, Action of natural products on p2 receptors: a reinvented era for drug discovery, Molecules 17 (2012) 13009-13025.

[37] R.A. North, M.F. Jarvis, P2X receptors as drug targets, Mol. Pharmacol. 83 (2013) 759-769.

[38] D. Dheer, V. Singh, R. Shankar, Medicinal attributes of 1,2,3-triazoles: Current developments, Bioorg. Chem. 71 (2017) 30-54.

[39] V.F. Ferreira, D.R. da Rocha, F.C. da Silva, P.G. Ferreira, N.A. Boechat, J.L. Magalhães, Novel 1H-1,2,3-, 2H-1,2,3-, 1H-1,2,4- and 4H-1,2,4-triazole derivatives: a patent review (2008 - 2011), Expert Opin. Ther. Pat. 23 (2013) 319-331.

[40] F.C. da Silva, M.C.B.V. de Souzaa, I.I.P. Frugulhetti, H.C. Castro, S.L. de O. Souza, T.M.L. de Souza, D.Q. Rodrigues, A.M.T. Souza, Synthesis, HIV-RT inhibitory activity and SAR of 1-benzyl-1H-1,2,3-triazole derivatives of carbohydrates, Eur. J. Med. Chem. 44 (2009) 373-383.

[41] C. Im, S.N. Maiti, R.G. Micetich, M. Daneshtalab, K. Atchison, O.A. Phillips, C. Kunugita, Synthesis and beta-lactamase inhibitory activity of 6-[(1-heteroarylthioethyl-1,2,3-triazol-4-yl)-methylene]penam sulfones, J. Antibiot. 47 (1994) 1030-1040.

[42] S. Palhagen, R. Canger, O. Henriksen, J.A. van Parysd, M.-E. Rivièree, M.A. Karolchyk, Rufinamide: a double-blind, placebo-controlled proof of principle trial in patients with epilepsy, Epilepsy Res. 43 (2001) 115-124.

[43] A.C. Cunha, J.M. Figueiredo, J.L.M. Tributino, A.L.P. Miranda, H.C. Castro, R.B. Zingali, C.A.M. Fraga, M.C.B.V. de Souza, V.F. Ferreira, Antiplatelet properties of novel N-substituted-phenyl-1,2,3-triazole-4-acylhydrazone derivatives, Bioorg. Med. Chem. 11 (2003) 2051-2059.

[44] A.K. Jordão, V.F. Ferreira, E.S. Lima, M.C.B.V. de Souza, E.C.L. Carlos, H.C. Castro, R.B. Geraldo, C.R. Rodrigues, M.C.B. Almeida, A.C. Cunha, Synthesis, antiplatelet and in silico evaluations of novel N-substituted-phenylamino-5-methyl-1H-1,2,3-triazole-4-carbohydrazides, Bioorg. Med. Chem. 17 (2009) 3713-3719.

[45] R. Menegatti, A.C. Cunha, V.F. Ferreira, E.F.R Perreira, A. El-Nabawi, A.T. Eldefrawi, E.X. Albuquerque, G. Neves, S.M.K Rates, C.A.M Fraga, E.J. Barreiro, Design, synthesis and pharmacological profile of novel dopamine D2 receptor ligands, Bioorg. Med. Chem. 11 (2003) 4807-4813.

[46] G. Biagi, G. Dell'Omodarme, M. Ferretti, I. Giorgi, O. Livi, V. Scartoni, E. Tiscione, Studies on 1,2,3-triazole derivatives as in vitro inhibitors of prostaglandin synthesis, Farmaco 45 (1990) 1181-1192.

[47] N. Boechat, V.F. Ferreira, S.B. Ferreira, M.L.G. Ferreira, F.C. da Silva, M.M. Bastos, M.S. Costa, M.C.S. Lourenço, A.C. Pinto, A.U. Krettli, A.C. Aguiar, B.M. Teixeira, N.V. da Silva, P.R.C. Martins, F.A.F.M. Bezerra, A.L.S. Camilo, G.P. da Silva, C.C.P. Costa, Novel 1,2,3-Triazole Derivatives for Use against Mycobacterium tuberculosis H37Rv (ATCC 27294) Strain, J. Med. Chem. 54 (2011) 5988-5999.

[48] A.K. Jordão, P.C. Sathler, V.F. Ferreira, V.R. Campos, M.C.B.V. de Souza, H.C. Castro, A. Lannes, A. Lourenco, C.R. Rodrigues, Synthesis, antitubercular activity, and SAR study of N-substituted-phenylamino-5-methyl-1H-1,2,3-triazole-4-carbohydrazides, Bioorg. Med. Chem. 19 (2011) 5605-5611.

[49] M.L. Ferreira, M.V.N. de Souza, S.M.S.V. Wardell, J.L. Wardell, T.R.A. Vasconcelos, V.F. Ferreira, M.C.S. Lourenço, Synthesis and Antitubercular Evaluation of New Bis-1,2,3-Triazoles Derived from D-Mannitol, J. Carbohydr. Chem. 29 (2010) 265-274.

[50] D.T.G. Gonzaga, D.R. Rocha, F.C. da Silva, V.F. Ferreira, Recent advances in the synthesis of new antimycobacterial agents based on the 1H-1,2,3-triazoles, Curr. Top. Med. Chem. 13 (2013) 2850-2865.

[51] A.K. Jordão, V.F. Ferreira, T.M.L. Souza, G.G.S. Faria, V. Machado, J.L. Abrantes, M.C.B.V. de Souza, A.C. Cunhaa, Synthesis and anti-HSV-1 activity of new 1,2,3-triazole derivatives, Bioorg. Med. Chem. 19 (2011) 1860-1865.

[52] E.N. da Silva Júnior, M.A.B.F. de Moura, A.V. Pinto, M.C.F.R. Pinto, M.C.B.V. de Souza, A.J. Araújo, C. Pessoa, L.V. Costa-Lotufo, R.C. Montenegro, M.O. de Moraes, V.F. Ferreira, M.O.F. Goulart, Cytotoxic, trypanocidal activities and physicochemical parameters of nor-beta-lapachone-based 1,2,3-triazoles, J. Braz. Chem. Soc. 20 (2009) 635-643.

[53] S.B. Ferreira, S.B. Ferreira, M.S. Costa, N. Boechat, R.J.S. Bezerra, M.S. Genestra, M.M. Canto-Cavalheiro, W.B. Kover, V.F. Ferreira, Synthesis and evaluation of new difluoromethyl azoles as antileishmanial agents, Eur. J. Med. Chem. 42 (2007) 1388-1395.

[54] I. da Silva, P.R.C. Martins, E.G. da Silva, S.B. Ferreira, V.F. Ferreira, K.R.C. da Costa, M.C. de Vasconcellos, E.S. Lima, F.C. da Silva, Synthesis of 1H-1,2,3-triazoles and study of their antifungal and cytotoxicity activities, Med. Chem. 9 (2013) 1085-1090.

[55] S.B. Ferreira, A.C.R. Sodero, M.F.C. Cardoso, E.S. Lima, C.R. Kaiser, F.P. SilvaJr., V.F. Ferreira Synthesis, biological activity, and molecular modeling studies of 1H-1,2,3-triazole derivatives of carbohydrates as alpha-glucosidases inhibitors, J. Med. Chem. 53 (2010) 2364-2375.

[56] D.T.G. Gonzaga, M.R Senger, F.C. da Silva, V.F. Ferreira, F.P.S. Junior, 1-Phenyl-1H- and 2-phenyl-2H-1,2,3-triazol derivatives: design, synthesis and inhibitory effect on alpha-glycosidases. Eur. J. Med. Chem. 74 (2014) 461-476.

[57] W.A. Carroll, D.M. Kalvin, A.P. Medrano, A.S. Florjancic, Y. Wang, D.L. Donnelly-Roberts, M.T. Namovic, G. Grayson, P. Honoré, M.F. Jarvis, Novel and potent 3-(2,3-dichlorophenyl)-4-(benzyl)-4H-1,2,4-triazole P2X7antagonists, Bioorg. Med. Chem. Lett. 17 (2007) 4044-4048.

[58] W.A. Carroll, D.L. Donnelly-Roberts, M.F. Jarvis, Selective P2X7receptor antagonists for chronic inflammation and pain, Purinergic Signal. 5 (2009) 63-73.

[59] A.S. Florjancic, S. Peddi, A. Perez-Medrano, B. Li, M.T. Namovic, G. Grayson, D.L. Donnelly-Roberts, M.F. Jarvis, W.A. Carroll, Synthesis and in vitro activity of 1-(2,3-dichlorophenyl)-N-(pyridin-3-ylmethyl)-1H-1,2,4-triazol-5-amine and 4-(2,3-dichlorophenyl)-N-(pyridin-3-ylmethyl)-4H-1,2,4-triazol-3-amine P2X7 antagonists, Bioorg. Med. Chem. Lett. 18 (2007) 2089-2092.

[60] D.L. Donnelly-Roberts, M.T. Namovic, P. Han, M.F. Jarvis, Mammalian P2X7 receptor pharmacology: comparison of recombinant mouse, rat and human P2X7 receptors, Br. J. Pharmacol. 157 (2009) 1203-1214.

[61] R.X. Faria, C.M. Cascabulho, R.A. Reis, L.A. Alves Large-conductance channel formation mediated by P2X7 receptor activation is regulated through distinct intracellular signaling pathways in peritoneal macrophages and 2BH4 cells, Naunyn Schmiedebergs Arch Pharmacol. 382 (2010) 73-87.

[62] J.B. Houston. Utility of in vitro drug metabolism data in predicting in vivo metabolic clearance. Biochem. Pharmacol. 47 (1994)1469-1479.

[63] T.A. Halgren, Merck Molecular Force Field I. basis, form, scope, parameterization, and performance of MMFF94, J. Comp. Chem. 17 (1996) 490-519.

[64] G.B. Rocha, R.O. Freire, A.M. Simas, J.J.P. Stewart, RM1: A Reparameterization of AM1 for H, C, N, O, P, S, F, Cl, Br and I, J. Comp. Chem. 27 (2006) 1101-1111.

[65] C. Lee, W. Yang, R.G. Parr, Development of the Colle-Salvetti correlation-energy formula into a functional of the electron density, Phys. Rev. B 37 (1988) 785-789.

[66] A.D. Becke, Density-functional thermochemistry. III. The role of exact exchange, J. Chem. Phys. 98 (1993) 5648-5652.

[67] W. Kohn, A.D. Becke, R.G. Parr, Density Functional Theory of Electronic Structure, J. Phys. Chem. 100 (1996) 12974-12980.

[68] D. Seeliger, B.L. de Groot, Ligand docking and binding site analysis with PyMOL and Autodock/Vina, J. Comput. Aided Mol. Des. 24 (2010) 417-422.

[69] O. Trott, A.J. Olson, AutoDock Vina: improving the speed and accuracy of docking with a new scoring function, efficient optimization, and multithreading, J. Comput. Chem. 31 (2010) 455-461.

[70] A. Karasawa, T. Kawate, Structural basis for subtype-specific inhibition of the P2X7 receptor, eLife 5 (2016) e22153.

[71] M. Bodnar, H. Wang, T. Riedel, S. Hintze, E. Kato, G. Fallah, H. Gröger-Arndt, R. Giniatullin, M. Grohmann, R. Hausmann, G. Schmalzing, P. Illes, P. Rubini, Amino acid residues constituting the agonist binding site of the human P2X3 receptor, J. Biol. Chem. 286 (2011) 2739-2749.

[72] L.H. Jiang, F. Rassendren, A. Surprenant, R.A. North, Identification of amino acid residues contributing to the ATP-binding site of a purinergic P2X receptor, J. Biol. Chem. 275 (2000) 34190-34196.

[73] D.T.G. Gonzaga, M.R. Senger, F.C. da Silva, V.F. Ferreira, F.P.S. Junior, 1-Phenyl-1H- and 2-phenyl-2H-1,2,3-triazol derivatives: design, synthesis and inhibitory effect on alpha-glycosidases, Eur. J. Med. Chem. 74 (2014) 461-476.

[74] V.V. Rostovtsev, L.G. Green, V.V. Fokin, K.B. Sharpless, A Stepwise Huisgen Cycloaddition Process: Copper(I)-Catalyzed Regioselective Ligation of Azides and Terminal Alkynes, Angew. Chem. Int. Ed. 41 (2002) 2596-2599.

[75] J.R. Gever, D.A. Cockayne, M.P. Dillon, G. Burnstock, A.P. Ford, Pharmacology of P2X channels, Pflugers Archiv. 452 (2006) 513-537.

[76] C. Coddou, Z. Yan, T. Obsil, J.P. Huidobro-Toro, S.S. Stojilkovic, Activation and regulation of purinergic P2X receptor channels, Pharmacol. Rev. 63 (2011) 641-683.

[77] A. Perez-Medrano, D.L. Donnelly-Roberts, A.S. Florjancic, D.W. Nelson, T. Li, M.T. Namovic, S. Peddi, C.R. Faltynek, M.F. Jarvis, W.A. Carroll, Synthesis and in vitro activity of N-benzyl-1-(2,3-dichlorophenyl)-1H-tetrazol-5-amine P2X7 antagonists, Bioorg. Med. Chem. Lett. 21 (2011) 3297-3300.

[78] B. Davies, T. Morris, Physiological parameters in laboratory animals and humans. Pharm Res. 10 (1993) 1093-1095.

[79] L.E. Ziganshina, A.U. Ziganshin, C.H. Hoyle, G. Burnstock, Acute paw oedema formation induced by ATP: re-evaluation of the mechanisms involved, Inflamm. Res. 45 (1996) 96-102.

[80] I. Posadas, M. Bucci, F. Roviezzo, A. Rossi, L. Parente, L. Sautebin, G. Cirino, Carrageenan-induced mouse paw oedema is biphasic, age-weight dependent and displays differential nitric oxide cyclooxygenase-2 expression, Br J Pharmacol. 142 (2004) 331-338.

[81] L. Stokes, L.-H. Jiang, L. Alcaraz, J. Bent, K. Bowers, M. Fagura, M. Furber, M. Mortimore, M. Lawson, J. Theaker, C. Laurent, M. Braddock, A. Surprenant, Characterization of a selective and potent antagonist of human P2X(7) receptors, AZ11645373, Br. J. Pharmacol. 149 (2006) 880-887.

[82] E.F. Pettersen, T.D. Goddard, C.C. Huang, G.S. Couch, D.M. Greenblatt, E.C. Meng, T.E. Ferrin, UCSF Chimera-a visualization system for exploratory research and analysis. J. Comput. Chem. 25 (2004)1605-1612.

[83] E.A. Caseley, S.P. Muench, C.W. Fishwick, L.-H. Jiang, Structure-based identification and characterisation of structurally novel human P2X7 receptor antagonists. Biochem. Pharmacol. 116 (2016) 130-139.

[84] M. Barniol-Xicota, S.-H. Kwak, S.-D. Lee, E. Caseley, E. Valverde, L.-H. Jiang, Y.-C. Kim, S. Vázquez, Escape from adamantane: Scaffold optimization of novel P2X7 antagonists featuring complex polycycles. Bioorg. Med. Chem. Lett. 27 (2017) 759-763.

[85] R.A. North, Molecular physiology of P2X receptors. Physiol. Rev. 82 (2002) 1013-1067.

[86] X. Chen, B. Pierce, W. Naing, M.L. Grapperhaus, D.P. Phillion, Discovery of 2-chloro-N-((4,4-difluoro-1-hydroxycyclohexyl)methyl)-5-(5-fluoropyrimidin-2-yl)benzamide as a potent and CNS penetrable P2X7 receptor antagonist, Bioorg. Med. Chem. Lett. 20 (2010) 3107-3111.

[87] D.A. Rudolph, J. Alcazar, M.K. Ameriks, A.B. Anton, H. Ao, P. Bonaventure, N.I. Carruthers, C.C. Chrovian, M.D. Angelis, B. Lord, J.C. Rech, Q. Wang, A. Bhattacharya, J.I. Andres, M.A.

Letavica, Novel methyl substituted 1-(5,6-dihydro-[1,2,4]triazolo[4,3-a]pyrazin-7(8H)-yl)methanones are P2X7 antagonists, Bioorg. Med. Chem. Lett. 25 (2015) 3157-3163.

[88] B.M. Savall, D. Wu, M.D. Angelis, N.I. Carruthers, H. Ao, Q. Wang, B. Lord, A. Bhattacharya, M.A. Letavic, Synthesis, SAR, and Pharmacological Characterization of Brain Penetrant P2X7 Receptor Antagonists, ACS Med. Chem. Lett. 24 (2015) 671-676.

[89] M.H. Abdi, P.J. Beswick, A. Billinton, L.J. Chambers, A. Charlton, S.D. Collins, K.L. Collis, D.K. Dean, E. Fonfria, R.J. Gleave, C.L. Lejeune, D.G. Livermore, S.J. Medhurst, A.D. Michel, A.P. Moses, L. Page, S. Patel, S.A. Roman, S. Senger, B. Slingsby, J.G.A. Steadman, A.J. Stevens, D.S. Walter, Discovery and structure-activity relationships of a series of pyroglutamic acid amide antagonists of the P2X7 receptor, Bioorg. Med. Chem. Lett. 20 (2010) 5080-5084.

[90] C. Csölle, B. Sperlágh, Peripheral origin of IL-1bproduction in the rodent hippocampus under in vivo systemic bacterial lipopolysaccharide (LPS) challenge and its regulation by P2X(7) receptors, J. Neuroimmunol. 219 (2010) 38-46.

[91] M. Barberà-Cremades, A. Baroja-Mazo, A.I. Gomez, F. Machado, F. Di Virgilio, P. Pelegrín, P2X7 receptor-stimulation causes fever via PGE2 and IL-1brelease, FASEB J. 26 (2012) 2951-2962.

[92] C. Virginio, D. Church, R.A. North, A. Surprenant Effects of divalent cations, protons and calmidazolium at the rat P2X7 receptor, Neuropharmacology 36 (1997) 1285-1294.

[93] N.-i.-H. Syed, C. Kennedy, Pharmacology of P2X receptors, WIREs Membr Transp Signal 1 (2012) 16-30.

[94] C.C. Chrovian, A. Soyode-Johnson, H. Ao, G.M. Bacani, N.I. Carruthers, B. Lord, L. Nguyen, J.C. Rech, Q. Wang, A. Bhattacharya, M.A. Letavic, Novel Phenyl-Substituted 5,6-Dihydro-[1,2,4]triazolo[4,3-a]pyrazine P2X7 Antagonists with Robust Target Engagement in Rat Brain, ACS Chem. Neurosci. 7 (2016) 490-497.

[95] F. Lopez-Tapia, K.A.M. Walker, C. Brotherton-Pleiss, J. Caroon, D. Nitzan, L. Lowrie, S. Gleason, S.-H. Zhao, J. Berger, D. Cockayne, D. Phippard, R. Suttmann, W.L. Fitch, D. Bourdet, P. Rege, X. Huang, S. Broadbent, C. Dvorak, J. Zhu, P. Wagner, F. Padilla, B. Loe, A. Jahangir, A. Alker, Novel Series of Dihydropyridinone P2X7 Receptor Antagonists, J. Med. Chem. 58 (2015) 8413-8426.

[96] A.K. Clark, A.A. Staniland, F. Marchand, T.K.Y. Kaan, S.B. McMahon, M. Malcangio, P2X7-dependent release of interleukin-1beta and nociception in the spinal cord following lipopolysaccharide, J Neurosci. 30 (2010) 573-582.

Triazoles inhibit mP2X7R function *in vitro*.

Triazoles inhibit IL-1beta release mediated by P2X7R activation.

Triazoles inhibit hP2X7R *in vitro*.

Triazoles inhibit acute inflammatory response *in vivo*.

Triazoles potentially are competitive P2X7R antagonist.